

Cadherin-dependent filopodia control preimplantation embryo compaction

Juan Carlos Fierro-González^{1,2}, Melanie D. White^{1,2}, Juan Carlos Silva¹ and Nicolas Plachta^{1,3}

Compaction of the preimplantation embryo is the earliest morphogenetic process essential for mammalian development, yet it remains unclear how round cells elongate to form a compacted embryo. Here, using live mouse embryo imaging, we demonstrate that cells extend long E-cadherin-dependent filopodia on to neighbouring cells, which control the cell shape changes necessary for compaction. We found that filopodia extension is tightly coordinated with cell elongation, whereas retraction occurs before cells become round again before dividing. Laser-based ablations revealed that filopodia are required to maintain elongated cell shapes. Moreover, molecular disruption of the filopodia components E-cadherin, α - and β -catenin, F-actin and myosin-X prevents cells from elongating and compacting the embryo. Finally, we show that early filopodia formation triggered by overexpressing myosin-X is sufficient to induce premature compaction. Our findings establish a role for filopodia during preimplantation embryonic development and provide an *in vivo* context to investigate the biological functions of filopodia in mammals.

Following fertilization, mouse and human embryos undergo a series of cleavage divisions producing relatively round cells. Starting at the 8-cell stage, compaction marks the beginning of a morphogenetic process essential to prepare the embryo for implantation^{1,2}. During compaction, cells flatten their membranes against each other, allowing them to increase cell–cell contact and establish the first epithelium-like structure. Failure of compaction results in non-viable embryos and the timing of compaction is inversely correlated with implantation success of human embryos derived from *in vitro* fertilization^{3–5}. Despite significant progress in understanding how cells acquire lineage identities in compacted embryos^{6,7}, the mechanisms controlling earlier morphological changes required for compaction remain poorly understood.

As preimplantation embryos are encapsulated by the zona pellucida, compaction is thought to depend on cell–cell interactions mediated by adhesion molecules such as E-cadherin^{8,9} (E-cad). Mouse embryos show compaction defects following treatment with E-cad antibodies¹⁰ or E-cad (*Cdh1*) deletion^{8,9}. Through dynamic interactions with intracellular catenins, E-cad regulates actin filaments (F-actin) and cell shape in various contexts^{11,12}. Here, to investigate how E-cad dynamics relate to cell shape changes during compaction we used confocal time-lapse imaging to follow E-cad fused to GFP (E-cad–GFP) in intact preimplantation mouse embryos. This approach allowed us to identify E-cad-dependent filopodia and we demonstrate an unknown role for these structures in controlling cell shape during compaction.

RESULTS

Identification of E-cad-expressing filopodia during mouse embryo compaction

To follow E-cad dynamics in living embryos undergoing compaction we microinjected RNA encoding E-cad–GFP into one cell at the 2-cell stage (Fig. 1a). The resultant mosaic embryos enabled us to visualize E-cad–GFP-labelled cellular structures interacting with unlabelled cells. Four-dimensional (4D) imaging (x , y , z and time) was performed using sensitive light detectors and optimized confocal spatiotemporal sampling conditions to reduce laser intensity (see Supplementary Information) as embryos underwent compaction. E-cad–GFP was present throughout the cell membrane, including the apical domain, and was enriched at regions of cell–cell contacts, typically referred to as adherens junctions. Analysis of 4D reconstructions, led to the identification of long filopodia-like cell protrusions containing E-cad–GFP (Fig. 1b,c). These structures were on average $10.9 \pm 0.8 \mu\text{m}$ long (Supplementary Fig. 1). They extended from the border between the adherens junctions and apical membrane (hereafter referred to as apical border) onto the apical membrane of neighbouring cells (Fig. 1b–d and Supplementary Fig. 1). E-cad filopodia were undetectable before embryos reached the 8-cell stage and started compaction, and were absent during the 16- to 32-cell stage when embryos appeared fully compacted (Supplementary Fig. 1).

¹European Molecular Biology Laboratory, Australian Regenerative Medicine Institute, Level 1 Building 75, Monash University, Victoria 3800, Australia. ²These authors contributed equally to this work.

³Correspondence should be addressed to N.P. (e-mail: nicolas.plachta@emblaaustralia.org)

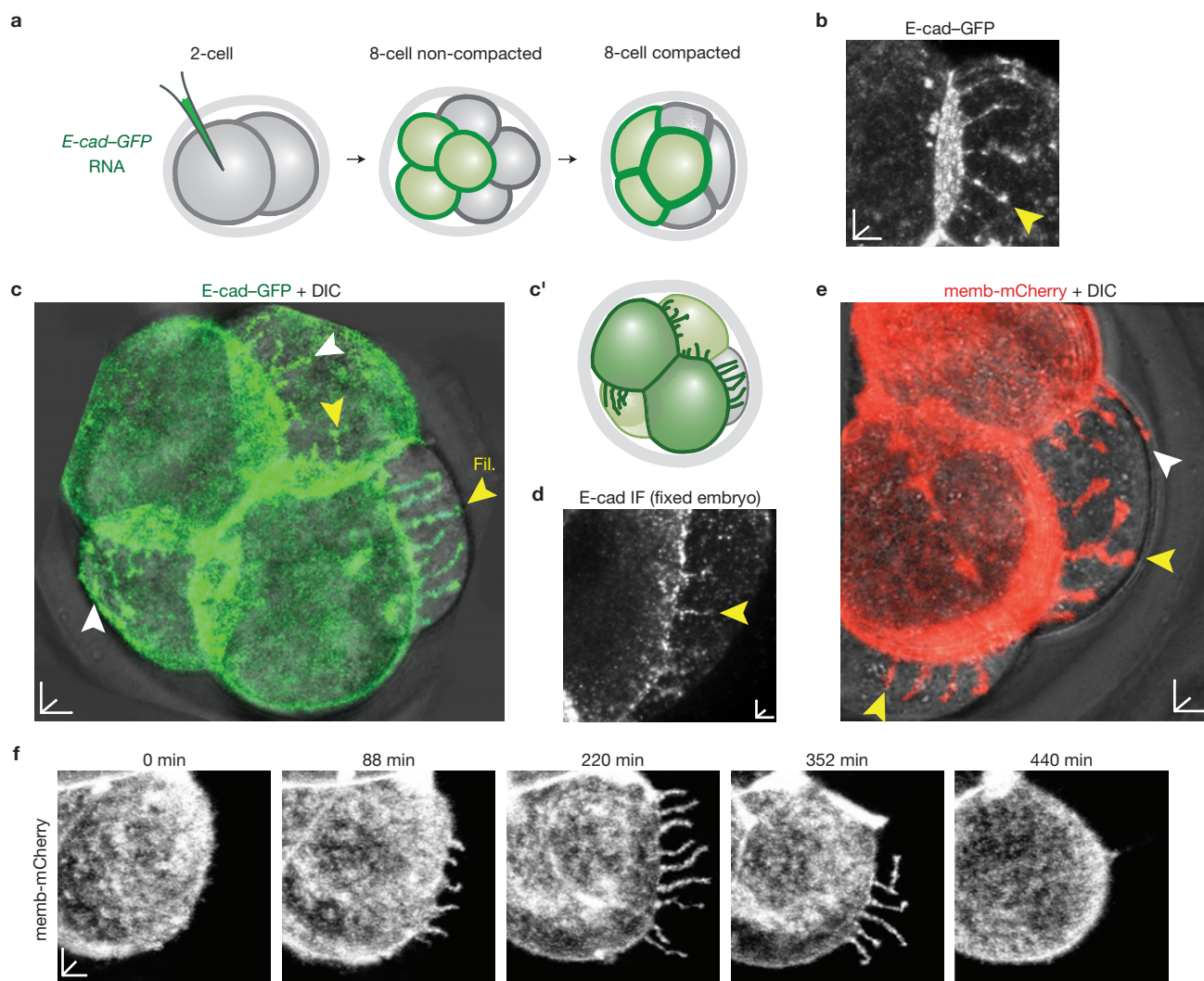


Figure 1 E-cad filopodia form during mouse embryo compaction. **(a)** Microinjection of RNA into one cell at the 2-cell stage allows visualization of E-cad-GFP in half of the cells of the embryo during compaction. **(b,c)** Microinjected live 8-cell stage embryos expressing E-cad-GFP. In **b**, E-cad-GFP-labelled filopodia (arrow) extend from the apical border membrane region of a filopodia-forming cell (left) on top of the neighbouring cell apical membrane (right). In **c**, two cells show

E-cad-GFP-labelled filopodia (white and yellow arrowheads distinguish filopodia from each cell). **(c')** Schematic diagram of the embryo from **c**. **(d)** Detection of filopodia using E-cad antibodies. IF, immunofluorescence. **(e)** Membrane-targeted mCherry (memb-mCherry) labels *bona fide* E-cad filopodia extending from two cells (white and yellow arrowheads). **(f)** Selected time frames show extension and retraction of filopodia over time. Orthogonal scale bars, 5 μ m.

The specificity of E-cad filopodia was confirmed in non-microinjected freshly isolated embryos immunolabelled with E-cad antibodies (Fig. 1d). Furthermore, *bona fide* E-cad filopodia were also detectable in live embryos microinjected with RNA encoding membrane-targeted mCherry (memb-mCherry; Fig. 1e and Supplementary Fig. 1), expressing memb-mCherry and E-cad-GFP, or by differential interference contrast (DIC; Supplementary Fig. 1). In agreement with classic descriptions of filopodia as F-actin-rich structures^{13,14}, an F-actin-binding domain fused to GFP (Lifeact-GFP; ref. 15) labelled filopodia in live embryos, and in fixed embryos E-cad-immunolabelled filopodia co-localized with rhodamine-phalloidin revealing F-actin (Supplementary Fig. 1). We did not detect microtubules in filopodia in live embryos expressing GFP- α -tubulin, nor in fixed embryos immunolabelled with E-cad and α -tubulin antibodies (Supplementary Fig. 1).

Time-lapse imaging of embryo compaction (8- to 16-cell stage) revealed stereotypical patterns of filopodia distribution: $61 \pm 6\%$ of cells per embryo extended filopodia at varying times throughout compaction (hereafter referred to as filopodia-forming cells); these cells extended 5.6 ± 0.2 filopodia per neighbouring cell and they targeted 2.4 ± 0.3 neighbouring cells simultaneously (Figs 1b,c,e and 2 and Supplementary Fig. 1); filopodia extended and remained elongated over 303 ± 46 min ($n = 7$ embryos) and retracted over 60 ± 9 min ($n = 7$ embryos; Fig. 1f and Supplementary Videos 1 and 2). To assess the proportion and distribution of filopodia-forming cells relative to each other and to the rest of the cells within the same embryo, we used two-photon excitation (2PE) microscopy in embryos microinjected with E-cad-GFP at the 1-cell stage (Fig. 2). This approach allowed us to image the filopodia of every cell in the same embryo and confirmed a proportion of filopodia-forming cells per embryo of $56 \pm 2\%$ (Fig. 2g).

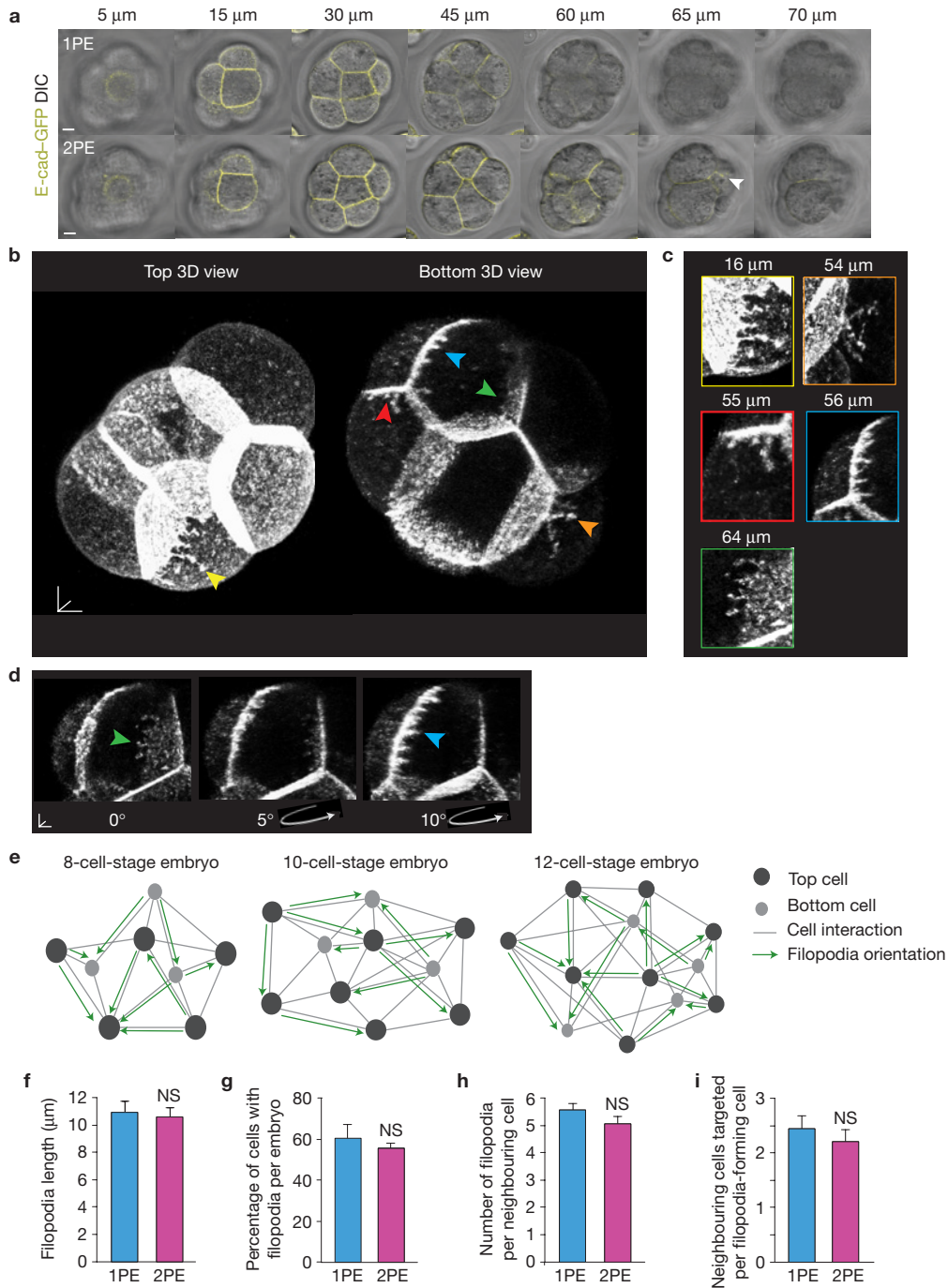


Figure 2 Filopodia distribution patterns imaged with two-photon excitation (2PE) microscopy. **(a)** 2PE microscopy allows visualization of every cell in a live 8-cell-stage embryo microinjected with E-cad-GFP RNA at the 1-cell stage. Images are selected Z scans with their approximate distance from the top of the same embryo using confocal (one-photon excitation, 1PE, top row) and 2PE (bottom row). With 1PE it is difficult to detect fluorescence beyond $\sim 60 \mu\text{m}$ in depth, but not with 2PE: the white arrowhead shows filopodia detected at $>60 \mu\text{m}$ from the top of the embryo. **(b)** Selected top and bottom 2PE 3D reconstructions of the embryo shown in **a**. Only the proximal $\sim 60\%$ of the embryo is shown in each view to minimize noise. **(c)** Colour-coded insets show higher-magnification views of the filopodia shown by arrows in **b**. Their approximate distance from the top of the embryo is indicated. **(d)** The three images are examples of the same 3D reconstruction: cropped along the Z axis, rotated and viewed from different angles. Filopodia originating from a cell on the right side of the image are clearly visible in the left panel (arrow).

Rotating the 3D reconstruction slightly allows visualization of filopodia originating from a cell on the left side. **(e)** Schematic representations show the distribution patterns of filopodia-forming cells in the same embryo. The three examples show embryos at the 8-, 10- and 12-cell stages imaged and analysed as described above. Circles depict cells. Grey lines depict direct cell-cell contact with neighbouring cells. Green arrows depict filopodia extensions and their orientation. The distribution patterns of filopodia in each embryo are in agreement with the main stereotypical patterns of filopodia formation described in our study (see Results). **(f–i)** Quantitative analysis of filopodia length **(f)**, the percentage of filopodia-forming cells per embryo **(g)**, number of filopodia per neighbouring cell **(h)** and number of neighbouring cells per filopodia-forming cell **(i)** obtained using 1PE or 2PE. NS, not significant by *t*-test. Error bars represent s.e.m. Statistics source data and sample sizes for **f–i** can be found in the Methods and Supplementary Table 1. Horizontal and orthogonal scale bars, $5 \mu\text{m}$.

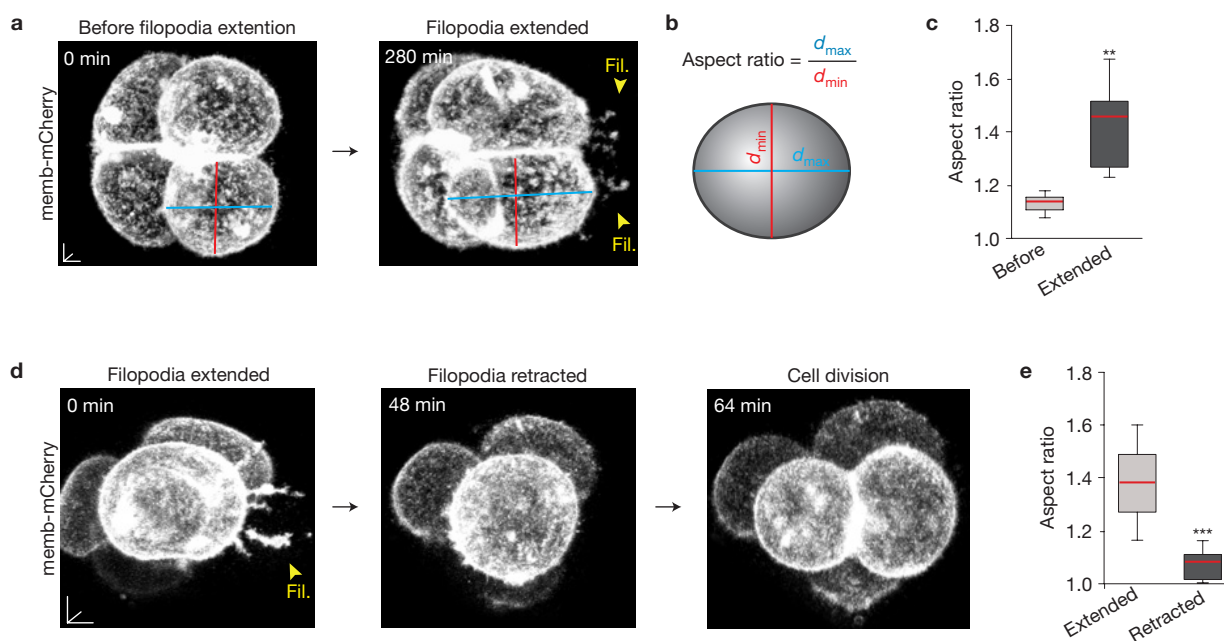


Figure 3 Filopodia extension–retraction dynamics are tightly coordinated with cell shape changes during compaction. **(a)** Selected time frames of a live embryo expressing memb-mCherry in half of its cells. Two cells show elongation of their apical border membrane following filopodia extension. **(b)** d_{\max} and d_{\min} are used to measure changes in aspect ratio. **(c)** Aspect ratio changes after filopodia extension ($n = 7$

cells). **(d)** Selected time frames show complete retraction of filopodia by an elongated cell, which becomes round before undergoing cell division. **(e)** Aspect ratio changes after filopodia retraction ($n = 9$ cells). *** $P < 0.001$, ** $P < 0.01$ by t -test. Error bars represent s.e.m. Statistics source data for **c** and **e** can be found in Supplementary Table 1. Orthogonal scale bars, 5 μ m.

In addition, cell distribution analyses revealed heterogeneous patterns in the distribution of filopodia-forming cells, without clustering of filopodia-forming cells in the same region of the embryo (Fig. 2b–e).

We also observed that cells never extended reciprocal filopodia on top of each other. The lack of reciprocal filopodia was confirmed by analysis of the 2PE data (Fig. 2b–e) and by experiments using confocal imaging, in which each cell of a 2-cell-stage embryo was microinjected with E-cad–GFP or memb-mCherry (Supplementary Fig. 2). In addition, we found that filopodia-forming cells always retracted their filopodia before undergoing cell division ($n = 20$ cells; Supplementary Video 3) and filopodia retraction was never observed without subsequent cell division (Supplementary Fig. 2). Moreover, cells receiving filopodia never divided when filopodia were extended over their membranes. Live embryo imaging further revealed that 69% of cells with filopodia underwent symmetric divisions, in which both daughter cells were allocated to the outer extraembryonic regions of the embryo, whereas the remaining 31% underwent asymmetric divisions, allocating one daughter cell to the outer and the other to the inside pluripotent region (Supplementary Fig. 3). This 7:3 ratio between symmetric/asymmetric divisions is expected during compaction^{16–18} and thus, our experiments suggest no a priori bias between the presence of filopodia and cell lineage allocation. Furthermore, tracking the progeny of a single cell microinjected at the 2-cell stage with memb-mCherry revealed that early blastomeres contribute a variable proportion of filopodia-forming cells during compaction (Supplementary Fig. 3), further indicating no obvious bias of 2-cell-stage blastomeres towards the generation of filopodia-forming cells. Together, these results established E-cad filopodia as a morphological feature of mouse embryo compaction.

Filopodia control cell shape during compaction

As E-cad filopodia appeared specifically during compaction, we reasoned that they may be associated with cell shape changes during this process. To test this, we microinjected memb-mCherry into one cell at the 2-cell stage, and followed filopodia dynamics and cell shape during compaction. Before extending filopodia, cells were relatively round, as demonstrated by aspect ratio measurements (d_{\max}/d_{\min}) close to 1 (Fig. 3a–c). However, following extension of filopodia, the apical border became elongated and the cell's aspect ratio increased (Fig. 3a–c). During compaction, cells became rounded again before division and retracted their filopodia as they reverted to a rounded shape (Fig. 3d,e). These experiments demonstrated a tight temporal coordination between filopodia extension–retraction dynamics and cell shape changes during compaction.

We next predicted that filopodia may provide tension to maintain the elongation of the apical border of filopodia-forming cells from which they extend. To address this, we expressed memb-mCherry in half of the embryo and performed multiphoton laser ablations targeting the initial 5 μ m from the base of filopodia. Following filopodia ablation, the angle of the apical border membrane adjacent to the filopodia base widened (mean angle of $81.6^\circ \pm 5.5^\circ$ pre-ablation, $131.9^\circ \pm 5.0^\circ$ post-ablation) and the region of membrane overlaying the neighbouring cell retracted (Fig. 4a–c). These changes were visible immediately after ablation, supporting the idea that ablating filopodia released tension maintaining the two neighbouring cells in close apposition. In these experiments we selected pairs consisting of a filopodia-forming cell expressing memb-mCherry and a memb-mCherry-negative neighbouring cell. This facilitated detection of labelled filopodia on top of non-fluorescent neighbouring structures.

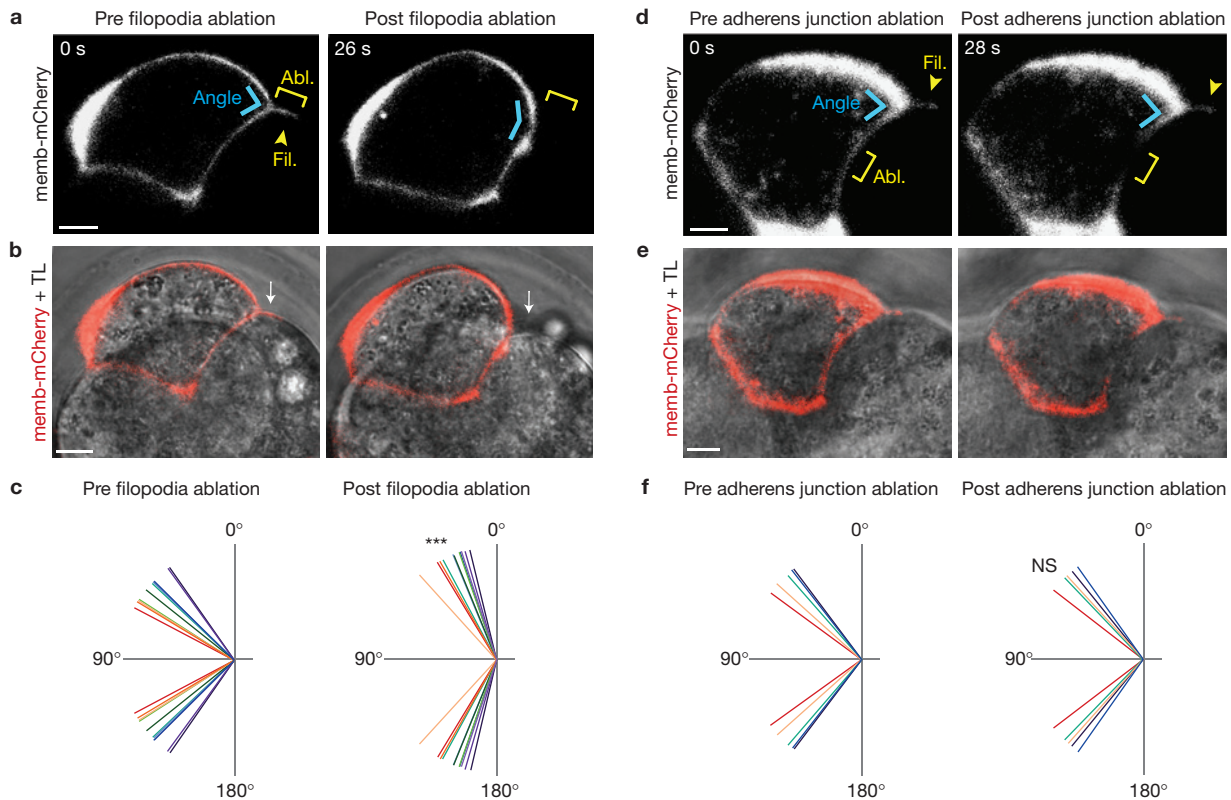


Figure 4 Filopodia laser-ablation perturbs cell shape. (a) Single focal plane of a cell expressing memb-mCherry in a live embryo. Immediately following filopodia laser-based ablation, the angle of the cell membrane in the apical border region widens (blue angle). (b) Transmitted light imaging shows a wider gap (arrow) between the two cells following filopodia laser ablation. (c) Apical border membrane angles before and after filopodia

laser ablations ($n = 11$ cells). (d–f) Unlike filopodia laser ablations, similar ablations performed along the adherens junction between filopodia-forming and neighbouring cells do not cause immediate changes in apical border membrane angles ($n = 5$ cells). *** $P < 0.001$; NS, not significant by t -test. Statistics source data for c,f can be found in Supplementary Table 1. Scale bars, $5\ \mu\text{m}$.

Nevertheless, using transmitted light we observed that following ablation the membrane region of the neighbouring cell where the filopodium attached also retracted and became rounded (arrow in Fig. 4b), further indicating a release of tension between cells. Adherens junctions are implicated in maintaining cell–cell adhesion^{12,19}. Unlike the effects of ablating filopodia, similar ablations performed at adherens junctions between filopodia-forming and neighbouring cells did not perturb the angle of the membrane border regions adjacent to filopodia (mean angle of $92.9^\circ \pm 6.5^\circ$ pre-ablation, $95.3^\circ \pm 5.4^\circ$ post-ablation; Fig. 4d–f), even when ablations caused fusion of the cells (Supplementary Fig. 4), suggesting that adherens junctions and filopodia affect different aspects of cell shape. Together, our time-lapse imaging and ablation experiments indicate that filopodia are important for cell shape changes during compaction.

Disrupting molecular components of filopodia affects cell shape and compaction

As physically disrupting filopodia indicated that these structures support the elongation of the cell's apical border, we predicted that molecular manipulations of filopodia components would affect cell shape during compaction. To test this we microinjected memb-mCherry with E-cad short interfering RNAs (siRNAs) into one cell at the 2-cell stage, to reduce E-cad expression in half of the embryo. By the onset of compaction, E-cad knockdown caused a reduction in the number of

filopodia per cell (Fig. 5a,c and Supplementary Fig. 5). Although E-cad knockdown cells formed fewer filopodia, these structures exhibited lengths of $9.6 \pm 0.9\ \mu\text{m}$ ($n = 14$ filopodia), extended and remained elongated over 256 ± 57 min ($n = 6$ embryos) and retracted over 53 ± 14 min ($n = 6$ embryos; Supplementary Fig. 5), similarly to control filopodia. Furthermore, knockdown cells failed to change shape, remaining rounded, as assessed by their aspect ratio, and did not integrate into the rest of the compacting embryo, formed by non-injected cells (Fig. 5b,d and Supplementary Fig. 5). We confirmed the specificity of the E-cad siRNA phenotype by a rescue experiment (Supplementary Fig. 5).

As it is well documented that interactions with α - and β -catenin (α -/ β -cat) control E-cad function¹⁹, we imaged live embryos co-expressing fusion proteins of either GFP- α -cat or β -cat-GFP, with E-cad-RFP, and found that both catenins co-localized with E-cad-RFP in filopodia (Supplementary Fig. 1). Moreover, similarly to inhibiting E-cad function, knockdown of endogenous α - and β -cat in half of the embryo led to reduced filopodia numbers and the knockdown cells remained rounded and did not integrate into the compacting embryo (Fig. 5a,b and Supplementary Fig. 5). Immunolabelling showed that both α - and β -cat siRNA downregulated E-cad membrane expression in regions filopodia normally extended from (Supplementary Fig. 5). These catenin results further support the view that an E-cad-dependent mechanism controls filopodia during compaction. Although manipulation of E-cad and catenins

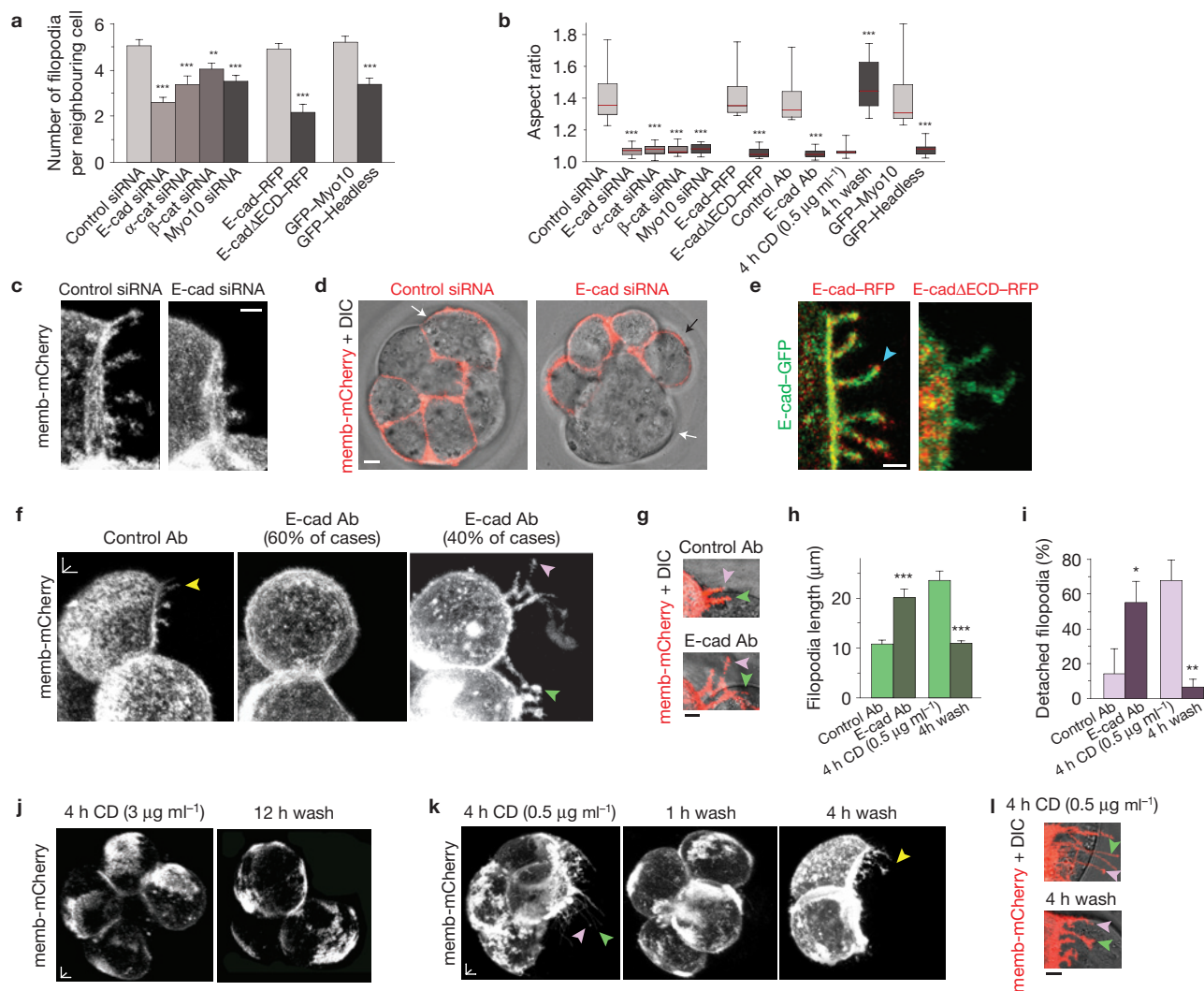


Figure 5 Molecular disruption of filopodia perturbs cell shape and compaction. **(a)** Molecular manipulation of filopodia components decreases filopodia number during compaction. **(b)** Manipulated cells remain rounded as assessed by their aspect ratio. CD, cytochalasin D. **(c,d)** Representative examples of reduced filopodia number **(c)** and failure to integrate into the compacting embryo **(d)** for cells microinjected with E-cad siRNAs and memb-mCherry (Fig. 6 and Supplementary Fig. 5 for the other examples of perturbed filopodia number and compaction). In **d**, white arrows show compacted and elongated cells, and the black arrow depicts a round cell that fails to integrate into the embryo. **(e)** E-cad-RFP is detected in filopodia (arrowhead), but E-cad Δ ECD-RFP fails to localize to the few filopodia that still form. **(f–i)** Blocking E-cad *trans* interactions with the DECMA-1 antibody

leads to no filopodia, or abnormally long (green arrowhead) and detached (pink arrowhead) filopodia. Arrowheads in control embryos show normal filopodia. **(j)** Cytochalasin D treatment at $3 \mu\text{g ml}^{-1}$ robustly prevents filopodia formation and compaction in all of the embryos analysed ($n = 11$ embryos) even after 12 h cytochalasin D washout (12 h wash). **(k,l)** Treatment with a lower cytochalasin D concentration ($0.5 \mu\text{g ml}^{-1}$) results in abnormally long (green arrowhead) and detached (pink arrowhead) filopodia, and cells remain rounded. Following 4 h cytochalasin D washout, cells extend normal filopodia and become elongated (see also **h,i**, and Supplementary Fig. 5). *** $P < 0.001$, ** $P < 0.01$, * $P < 0.05$ by *t*-test. Error bars indicate s.e.m. Statistics source data and exact sample sizes for **a,b,h,i** can be found in Methods and Supplementary Table 1. Horizontal and orthogonal scale bars, $5 \mu\text{m}$.

prevented embryos from compacting normally, some embryos eventually compacted after a varying delay of 6–36 h, possibly owing to compensatory mechanisms regulating compaction, which is in line with previous observations^{8,9}.

We reasoned that one function for E-cad in filopodia might be to mediate attachment to the neighbouring cell membrane through *trans* interactions. To test this, we used a dominant-negative E-cad protein with a truncated extracellular domain fused to RFP (E-cad Δ ECD-RFP), previously shown to interfere with *trans* interactions²⁰. We co-injected equal amounts of E-cad-GFP and E-cad Δ ECD-RFP RNA into one cell at the 2-cell stage and determined the effects on filopodia formation,

cell shape and compaction. Similarly to E-cad knockdown, expression of E-cad Δ ECD-RFP reduced the number of filopodia by the 8-cell stage and these cells also remained rounded with aspect ratios close to 1, and were unable to integrate into the compacting embryo (Fig. 5a,b,e and Supplementary Fig. 5). Unlike E-cad-GFP, E-cad Δ ECD-RFP failed to localize to the few filopodia that still form in these embryos (Fig. 5e) and was not enriched at adherens junctions (Supplementary Fig. 5), suggesting that *trans* interactions are required for E-cad accumulation in filopodia and adherens junctions. Control embryos in which E-cad-GFP was co-expressed with E-cad-RFP did not show defects in E-cad localization, filopodia number, cell shape or

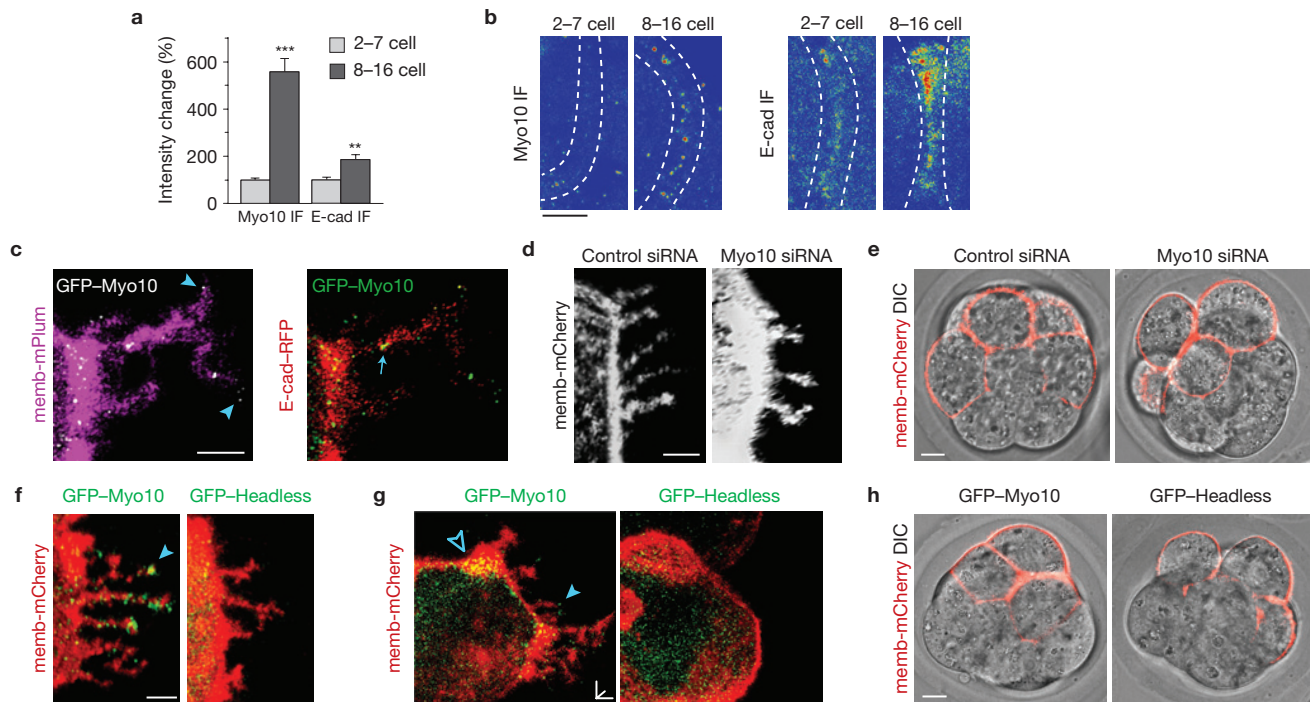


Figure 6 Myo10 is required for filopodia formation during compaction. (a) Endogenous Myo10 and E-cad fluorescence intensity increases at membrane regions where filopodia normally extend during compaction (8- to 16-cell stage) relative to earlier stages (2- to 7-cell stage; $n = 28$ membrane regions for Myo10 immunofluorescence at 2–7 cell, 28 for Myo10 immunofluorescence at 8–16 cell, 21 for E-cad immunofluorescence at 2–7 cell, 25 for E-cad immunofluorescence at 8–16 cell). *** $P < 0.001$; ** $P < 0.01$ by t -test. Error bars represent s.e.m. (b) Selected rainbow images represent the changes shown in a. (c) High-magnification view of filopodia in a live embryo microinjected with GFP-Myo10, memb-mPlum and E-cad-RFP. GFP-Myo10 puncta

localize along filopodia (arrow) and at their tips (arrowheads, see also f,g). (d,e) Myo10 knockdown causes a reduction in filopodia number (d) and prevents memb-mCherry-labelled cells from integrating into the rest of the compacting embryo (e). (f) GFP-Myo10 localizes along filopodia and their tips (arrowhead). GFP-Headless fails to localize to the few filopodia that still form. (g) GFP-Myo10, but not GFP-Headless, is enriched in membrane regions where filopodia normally extend (open arrowhead). (h) Cells microinjected with GFP-Headless fail to integrate into the compacting embryo and remain rounded. Statistics source data for a can be found in Supplementary Table 1. Horizontal and orthogonal scale bars, 5 μ m.

compaction (Fig. 5a,b,e and Supplementary Fig. 5). In agreement with these findings, acute extracellular treatment of 8-cell embryos with DECMA-1 E-cad antibodies previously shown to block *trans* interactions²¹ prevented filopodia formation in 60% of the embryos (Fig. 5f), and the remaining 40% formed abnormal filopodia that were longer and detached from the neighbouring cell apical membrane (Fig. 5f–i). Cells in antibody-treated embryos remained rounded exhibiting aspect ratios close to 1, and the embryos failed to compact compared with control embryos (Fig. 5b and Supplementary Fig. 5). This set of experiments shows that filopodia formation requires E-cad, and that filopodia length and attachment to the neighbouring cell membrane are probably mediated by E-cad *trans* interactions.

As F-actin regulates the filopodia cytoskeleton¹⁹, we determined the effect of treatment of 8-cell embryos with cytochalasin D on filopodia and compaction. Cytochalasin D treatment at 3 μ g ml⁻¹ depleted Lifeact-GFP fluorescence along the cell membrane and prevented filopodia formation completely (Fig. 5j). Cells remained rounded exhibiting an aspect ratio of 1.06 ± 0.02 ($n = 17$ cells from 6 embryos) and these embryos failed to compact (Fig. 5j and Supplementary Fig. 5), even following cytochalasin D washout (12 h wash). Treatment with a 6-fold lower cytochalasin D concentration (0.5 μ g ml⁻¹) reduced, but did not completely deplete, Lifeact-GFP fluorescence (Supplementary Fig. 6). These embryos extended a similar number of filopodia,

yet the treated filopodia were abnormally long and detached from the neighbouring cell membrane (Fig. 5h,i,k,l and Supplementary Fig. 6). In line with defects in filopodia, cells in embryos treated with 0.5 μ g ml⁻¹ cytochalasin D maintained aspect ratios close to 1 and the embryos failed to compact (Fig. 5b and Supplementary Fig. 5). This effect is consistent with earlier observations on mouse embryos treated with the same cytochalasin D concentration, which showed abnormal localization and length of microfilament structures and compaction defects^{22,23}. Following one hour of 0.5 μ g ml⁻¹ cytochalasin D washout, most filopodia fragmented, and 4 h later the cells extended filopodia showing normal length and attachment, exhibited significantly higher aspect ratios and formed a compacted embryo (Fig. 5b,h,i,k,l and Supplementary Figs 5 and 6). It is possible that the defects in filopodia length and attachment result from aberrant E-cad function or localization, because E-cad-GFP exhibited an abnormal distribution pattern in embryos treated with 0.5 μ g ml⁻¹ cytochalasin D, which was reverted following cytochalasin D washout (Supplementary Fig. 6). Finally, in agreement with filopodia not expressing α -tubulin, nocodazole-treated embryos formed filopodia and underwent normal compaction (Supplementary Fig. 6), in line with previous studies²⁴. Our results thus show that compaction is associated with the formation of filopodia exhibiting normal length and attachment and normal distribution of filopodia components such as E-cad.

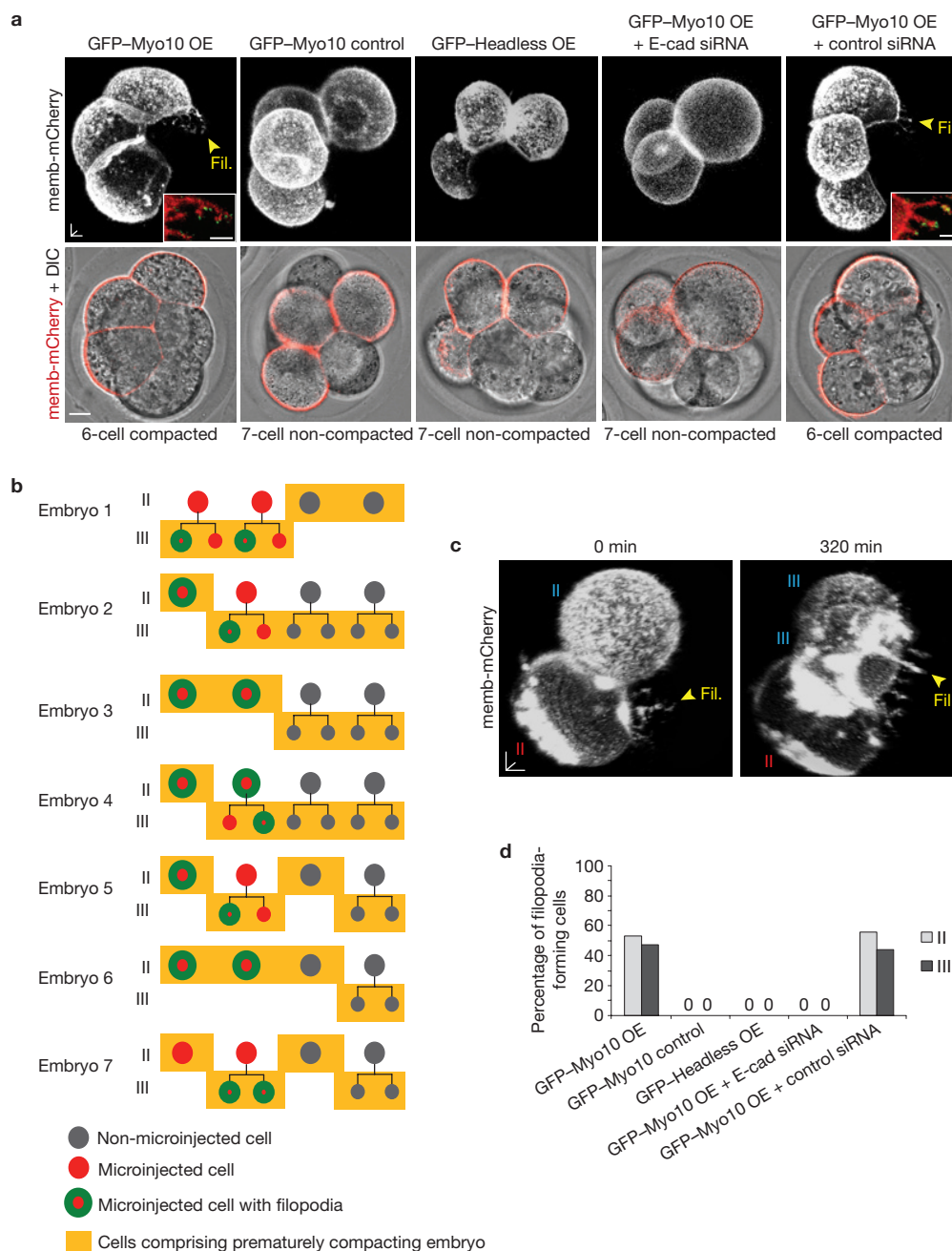


Figure 7 Premature filopodia formation induces early compaction. **(a)** Microinjection of a high concentration of GFP-Myo10 (overexpression, OE) with memb-mCherry RNA into one cell at the 2-cell stage induces premature filopodia formation (arrowhead) and embryo compaction (visible by DIC imaging) at the 5- to 7-cell stage. Lower GFP-Myo10 concentrations or GFP-Headless cannot induce filopodia and compaction. Co-injection with E-cad siRNAs suppresses the effect of GFP-Myo10 overexpression on filopodia formation and compaction. Insets show GFP-Myo10 expression along the prematurely induced filopodia ($n = 7$ embryos for GFP-Myo10 OE; 15 for GFP-Myo10 control; 11 for GFP-Headless OE; 20 for GFP-Myo10 OE + E-cad siRNA; 7 for GFP-Myo10 OE + control siRNA). **(b-d)** Overexpression of GFP-Myo10 can trigger filopodia formation in both second- and third-cleavage stage cells. **(b)** Schematic chart of seven representative embryos analysed for the experiments overexpressing GFP-Myo10 shown in **a**. We scored memb-mCherry-positive cells extending filopodia from 2-cell stage onwards, and determined whether these cells correspond to a second- or third-cleavage stage blastomere. During 5- to

7-cell stages, the embryos contain a mixture of second- and third-cleavage cells. Areas outlined in orange show the stage at which premature compaction was observed. Circles show all cells imaged. Colour codes indicate whether cells are non-microinjected (grey), microinjected (red) and extending filopodia (green-red circles). **(c)** Representative examples of embryo 5 (from **b**) at different time points. At time 0 min, the embryo contains two memb-mCherry-positive cells; both of these correspond to a second-cleavage stage and one of them is extending filopodia (arrow). At time 320 min, the second-stage cell has retracted its filopodia. The upper cell has divided into two third-cleavage stage cells. One of these cells is now extending filopodia (arrow). These examples show that both second- and third-cleavage stage cells can extend filopodia in the same embryo. Non-injected cells are not visualized in these examples. Roman numbers indicate cells corresponding to second- (II) or third- (III) cleavage stage. **(d)** Analysis of all embryos used in **a** confirms the ability of both second- and third-cleavage stage cells to extend filopodia when overexpressing GFP-Myo10. Horizontal and orthogonal scale bars, 5 μm .

Early filopodia formation causes premature compaction

To identify molecules required for induction of filopodia formation during compaction, we investigated myosin-X (Myo10). In cultured cells, this myosin localizes to filopodia and is important for their formation²⁵. Immunolabelling at different developmental stages revealed that Myo10 is expressed in embryos and its levels increased at apical border regions just before compaction (Fig. 6a,b). Furthermore, co-injection of Myo10 fused to GFP (GFP–Myo10), memb-mPlum and E-cad–RFP into one cell at the 2-cell stage revealed GFP–Myo10 puncta distributed along filopodia and enriched at filopodia tips (Fig. 6c), similarly to previous work in cultured cells²⁶. To test whether endogenous Myo10 is necessary for filopodia formation, we microinjected memb-mCherry with Myo10 siRNAs into one cell at the 2-cell stage. Similarly to reducing E-cad (Fig. 5a–d), knockdown of Myo10 decreased filopodia numbers and knockdown cells remained rounded and could not integrate into the compacting embryo (Figs 5a,b and 6d,e). We confirmed the specificity of the Myo10 siRNA phenotype by a rescue experiment (Supplementary Fig. 5). Moreover, a dominant-negative mutant Myo10 lacking the motor domain fused to GFP (GFP–Headless) failed to localize to filopodia tips, similarly to previous observations²⁷ (Fig. 6f), and showed reduced expression at apical border regions (Fig. 6g). In line with the knockdown approach, GFP–Headless also disrupted filopodia numbers and perturbed cell shape and compaction (Figs 5a,b and 6f–h). Although it remains unclear how Myo10 participates in filopodia formation²⁵, we noticed that 80% of GFP–Myo10 puncta co-localized with E-cad–RFP in apical border regions near the filopodia base ($n = 13$ filopodia), whereas only 11% of GFP–Myo10 puncta co-localized with E-cad–RFP along filopodia ($n = 22$ filopodia; Fig. 6c), suggesting that most Myo10 functions in filopodia are independent of direct interaction with E-cad. These experiments indicate that Myo10 is normally required for filopodia formation during compaction.

As disrupting filopodia by ablation and molecular manipulation prevented cell shape changes and compaction, we reasoned that inducing filopodia formation prematurely could promote early compaction. Expression of Myo10 at high concentration has been shown to induce filopodia formation in cultured cells²⁸. Overexpression of GFP–Myo10 in half of the embryo, but not of GFP–Headless, was sufficient to induce the premature formation of filopodia in 5- to 7-cell-stage embryos, and these embryos compacted prematurely (Fig. 7a). This effect was suppressed by co-injecting E-cad siRNAs with a high concentration of GFP–Myo10, suggesting a requirement for both molecules in filopodia formation and compaction (Fig. 7a). At the 5- to 7-cell stage, mouse embryos contain a mixture of second- and third-cleavage blastomeres^{6,7}. Overexpression of GFP–Myo10 could induce filopodia in both cell types (Fig. 7b–d), indicating that the potential to form filopodia is present before cells adopt a third-cleavage identity. These results indicate that Myo10 is essential for filopodia formation and support the view that E-cad-dependent filopodia play an active role in reshaping the embryo during compaction.

DISCUSSION

Studies from the late 1970s first noted diverse cell membrane protrusions in fixed preimplantation embryos^{23,29,30}. Here, we now demonstrate the presence of long filopodia that extend during compaction and are required for cell shape changes central to

this developmental process. These protrusions contain E-cad and components typically present in filopodia^{13,14}, including F-actin and Myo10. We propose an initial working model in which cells use filopodia to attach to the neighbouring cell apical membrane through E-cad *trans* interactions. Filopodia then maintain tension to elongate the apical membrane border over neighbouring cells, bringing the cells closer and facilitating compaction.

We found that ~60% of cells per embryo form filopodia. It is possible that these cells use filopodia to elongate their membrane and help neighbouring cells change shape by pulling the two cells closer. This idea is supported by our laser-ablation experiments that caused changes not only in filopodia-forming cells, but also in the adjacent cells, which became more rounded and separated (Fig. 4b). Similarly, when overexpressing GFP–Myo10, on average 40% of cells in each embryo formed filopodia, and the entire embryo developed a compacted morphology. This is in line with the idea that filopodia formation by some, but not all, cells in the embryo can promote compaction. In embryos where E-cad was disrupted in half of the cells using siRNAs, or by expression of an RFP-tagged dominant-negative E-cad protein with a truncated extracellular domain (E-cad Δ ECD–RFP), DIC imaging revealed normal elongation and flattening of the non-injected cells, and the region occupied by these cells exhibited a classic compacted morphology^{1,2} (Fig. 5d). It is likely that the non-injected cells can form normal filopodia and E-cad *trans* interactions with each other that help them undergo compaction, but not with the knockdown cells. Furthermore, we found that cells never extend reciprocal filopodia on top of each other, and filopodia-forming cells always retract their filopodia before dividing. Together, these patterns of filopodia formation could help prevent conflicting tension forces between neighbouring cells during compaction and facilitate membrane remodelling in cytokinesis. We also found that cells never divide while filopodia are extended on top of them. This suggests that in addition to maintaining tension, filopodia could further participate in compaction by enabling spatially restricted signalling to neighbouring cells, as reported for *Drosophila* cytonemes³¹. For example, signalling from filopodia could preclude simultaneous division of the filopodia-forming and neighbouring cells, which may be important to preserve packing of cells during compaction. Although it remains debated when and how cells adopt distinct developmental fates in the preimplantation embryo^{6,7,32}, our experiments revealed a heterogeneous distribution of filopodia-forming cells in the embryo and no direct association between filopodia formation and the allocation of cells to the pluripotent and extraembryonic lineages. Revealing mechanisms controlling whether or not cells form filopodia, and their relationship with cell division during compaction, is an important task for future investigation.

Thus far, filopodia have been implicated in key biological processes including morphogen signalling in *Drosophila* and avian embryos^{31,33}, cell migration, axonal pathfinding and cancer cell invasion^{13,14}. Our study establishes a role for filopodia in controlling cell shape during mouse embryo compaction and provides an *in vivo* context to investigate the roles of filopodia in mammals. Furthermore, as the timing of compaction in human embryos is associated with implantation success^{4,5}, a greater understanding of the role of filopodia in compaction may be clinically relevant for reproductive strategies based on *in vitro* fertilization. □

METHODS

Methods and any associated references are available in the [online version of the paper](#).

Note: Supplementary Information is available in the online version of the paper

ACKNOWLEDGEMENTS

We thank A. Yap, E. Jesudason, A. Fouras and J. Polo for comments on the manuscript; T. Bell for advice on laser ablations; S. Firth and I. Harper for help with imaging experiments; and R. Cheney, A. Yap and B. Henderson for sharing DNA constructs. N.P. is supported by ARC DP120104594 and DE120100794, NHMRC APP1052171 and Monash University Strategic and Interdisciplinary grants, and J.C.F.-G. by Wenner-Gren Foundations and Swedish Society for Medical Research Postdoctoral Fellowships.

AUTHOR CONTRIBUTIONS

J.C.F.-G. and M.D.W. designed and performed the experiments. J.C.S. performed embryo microinjections and manipulations. N.P. supervised the project. J.C.F.-G., M.D.W. and N.P. wrote the paper.

COMPETING FINANCIAL INTERESTS

The authors declare no competing financial interests.

Published online at www.nature.com/doi/10.1038/ncb2875

Reprints and permissions information is available online at www.nature.com/reprints

- Johnson, M. H., Maro, B. & Takeichi, M. The role of cell adhesion in the synchronization and orientation of polarization in 8-cell mouse blastomeres. *J. Embryol. Exp. Morphol.* **93**, 239–255 (1986).
- Johnson, M. H. & Ziomek, C. A. Induction of polarity in mouse 8-cell blastomeres: specificity, geometry, and stability. *J. Cell Biol.* **91**, 303–308 (1981).
- Landry, D. W., Zucker, H. A., Sauer, M. V., Reznik, M. & Wiebe, L. Hypocellularity and absence of compaction as criteria for embryonic death. *Regen. Med.* **1**, 367–371 (2006).
- Le Cruguel, S. *et al.* Early compaction at day 3 may be a useful additional criterion for embryo transfer. *J. Assist. Reprod. Genet.* **30**, 683–690 (2013).
- Skias, C. C., Jackson, K. V. & Racowsky, C. Early compaction on day 3 may be associated with increased implantation potential. *Fertil. Steril.* **86**, 1386–1391 (2006).
- Rossant, J. & Tam, P. P. Blastocyst lineage formation, early embryonic asymmetries and axis patterning in the mouse. *Development* **136**, 701–713 (2009).
- Zernicka-Goetz, M., Morris, S. A. & Bruce, A. W. Making a firm decision: multifaceted regulation of cell fate in the early mouse embryo. *Nat. Rev. Genet.* **10**, 467–477 (2009).
- Larue, L., Ohsugi, M., Hirchenhain, J. & Kemler, R. E-cadherin null mutant embryos fail to form a trophectoderm epithelium. *Proc. Natl Acad. Sci. USA* **91**, 8263–8267 (1994).
- Stephenson, R. O., Yamanaka, Y. & Rossant, J. Disorganized epithelial polarity and excess trophectoderm cell fate in preimplantation embryos lacking E-cadherin. *Development* **137**, 3383–3391 (2010).
- Dietrich, J. E. & Hiiragi, T. Stochastic patterning in the mouse pre-implantation embryo. *Development* **134**, 4219–4231 (2007).
- Michael, M. & Yap, A. S. The regulation and functional impact of actin assembly at cadherin cell–cell adhesions. *Semin. Cell Dev. Biol.* **24**, 298–307 (2013).
- Cavey, M. & Lecuit, T. Molecular bases of cell–cell junctions stability and dynamics. *Cold Spring Harb. Persp. Biol.* **1**, a002998 (2009).
- Gupton, S. L. & Gertler, F. B. Filopodia: the fingers that do the walking. *Sci. STKE* **2007**, re5 (2007).
- Mattila, P. K. & Lappalainen, P. Filopodia: molecular architecture and cellular functions. *Nat. Rev. Mol. Cell Biol.* **9**, 446–454 (2008).
- Riedl, J. *et al.* Lifeact: a versatile marker to visualize F-actin. *Nat. Methods* **5**, 605–607 (2008).
- Kaur, G. *et al.* Probing transcription factor diffusion dynamics in the living mammalian embryo with photoactivatable fluorescence correlation spectroscopy. *Nat. Commun.* **4**, 1637 (2013).
- Morris, S. A. *et al.* Origin and formation of the first two distinct cell types of the inner cell mass in the mouse embryo. *Proc. Natl Acad. Sci. USA* **107**, 6364–6369 (2010).
- Plachta, N., Bollenbach, T., Pease, S., Fraser, S. E. & Pantazis, P. Oct4 kinetics predict cell lineage patterning in the early mammalian embryo. *Nat. Cell Biol.* **13**, 117–123 (2011).
- Ratheesh, A. & Yap, A. S. A bigger picture: classical cadherins and the dynamic actin cytoskeleton. *Nat. Rev. Mol. Cell Biol.* **13**, 673–679 (2012).
- Nieman, M. T., Prudoff, R. S., Johnson, K. R. & Wheelock, M. J. N-cadherin promotes motility in human breast cancer cells regardless of their E-cadherin expression. *J. Cell Biol.* **147**, 631–644 (1999).
- Kobayashi, N., Ikesue, A., Majumdar, S. & Sahaan, T. J. Inhibition of E-cadherin-mediated homotypic adhesion of Caco-2 cells: a novel evaluation assay for peptide activities in modulating cell–cell adhesion. *J. Pharmacol. Exp. Ther.* **317**, 309–316 (2006).
- Johnson, M. H. & Maro, B. The distribution of cytoplasmic actin in mouse 8-cell blastomeres. *J. Embryol. Exp. Morphol.* **82**, 97–117 (1984).
- Sutherland, A. E. & Calarco-Gillam, P. G. Analysis of compaction in the preimplantation mouse embryo. *Dev. Biol.* **100**, 328–338 (1983).
- Maro, B. & Pickering, S. J. Microtubules influence compaction in preimplantation mouse embryos. *J. Embryol. Exp. Morphol.* **84**, 217–232 (1984).
- Kerber, M. L. & Cheney, R. E. Myosin-X: a MyTH-FERM myosin at the tips of filopodia. *J. Cell Sci.* **124**, 3733–3741 (2011).
- Berg, J. S., Derfler, B. H., Pennisi, C. M., Corey, D. P. & Cheney, R. E. Myosin-X, a novel myosin with pleckstrin homology domains, associates with regions of dynamic actin. *J. Cell Sci.* **113**, 3439–3451 (2000).
- Sousa, A. D., Berg, J. S., Robertson, B. W., Meeker, R. B. & Cheney, R. E. Myo10 in brain: developmental regulation, identification of a headless isoform and dynamics in neurons. *J. Cell Sci.* **119**, 184–194 (2006).
- Bohil, A. B., Robertson, B. W. & Cheney, R. E. Myosin-X is a molecular motor that functions in filopodia formation. *Proc. Natl Acad. Sci. USA* **103**, 12411–12416 (2006).
- Ducibella, T., Ukena, T., Karnovsky, M. & Anderson, E. Changes in cell surface and cortical cytoplasmic organization during early embryogenesis in the preimplantation mouse embryo. *J. Cell Biol.* **74**, 153–167 (1977).
- Calarco, P. G. & Epstein, C. J. Cell surface changes during preimplantation development in the mouse. *Dev. Biol.* **32**, 208–213 (1973).
- Roy, S., Hsiung, F. & Kornberg, T. B. Specificity of *Drosophila* cytonemes for distinct signaling pathways. *Science* **332**, 354–358 (2011).
- Wennekamp, S., Mesecke, S., Nedelec, F. & Hiiragi, T. A self-organization framework for symmetry breaking in the mammalian embryo. *Nat. Rev. Mol. Cell Biol.* **14**, 454–461 (2013).
- Sanders, T. A., Llagostera, E. & Barna, M. Specialized filopodia direct long-range transport of SHH during vertebrate tissue patterning. *Nature* **497**, 628–632 (2013).

METHODS

DNA and RNA work. The original sequence for mouse E-cad-GFP was provided by A. Yap, University of Queensland, mouse β -catenin by B. Henderson, University of Sydney, Lifeact-GFP by T. Hall, University of Queensland and bovine myosin-X by R. Cheney, UNC at Chapel Hill. Mouse α -catenin was obtained from Addgene (20139). All complementary DNA sequences were cloned into a pCS2-based vector and tagged constructs were generated by inserting full-length or deleted forms of the respective gene upstream or downstream of EGFP or mRFP. The truncated mutant E-cad Δ ECD-RFP contains a deletion of amino acids 107–625 of E-Cad (AAH98501) and Headless Myosin-X contains amino acids 641–2,062 of Myo10 (NP_062345). pCS2-membrane-mPlum was made by substituting mPlum for mCherry in pCS2-membrane-mCherry. RNA transcription and purification was performed using DNA constructs linearized with appropriate restriction enzymes and the mMESSAGE mMACHINE SP6 kit (Ambion) and RNeasy kit (Qiagen) following the manufacturer's instructions. RNA transcripts derived from each of the constructs described above were microinjected at the following concentrations: H2B-Cerulean at 15 ng μ l⁻¹; Lifeact-GFP (ref. 15) at 20 ng μ l⁻¹; memb-mCherry or memb-mPlum at 40 ng μ l⁻¹; GFP- α -tubulin, GFP- α -cat, β -cat-GFP, E-cad-GFP, E-cad-RFP or E-cad Δ ECD-RFP at 50 ng μ l⁻¹; GFP-Myo10 or GFP-Headless at 100 ng μ l⁻¹. For filopodia induction experiments, GFP-Myo10 or GFP-Headless overexpression was performed at 200 ng μ l⁻¹, and GFP-Myo10 control was injected at 100 ng μ l⁻¹. siRNA molecules (QIAGEN) for Scrambled (Ctrl_Allstars_1), E-cad (Mm_Cdh1_1 and Mm_Cdh1_6), α -cat (Mm_Catna1_1 and Mm_Catna1_6), β -cat (Mm_Catnb_2 and Mm_Catnb_3) and Myo10 (Mm_Myo10_1 and Mm_Myo10_4) were microinjected at a final concentration of 200 nM. For the rescue experiments, E-cad-GFP or GFP-Myo10 was microinjected at 100 ng μ l⁻¹, together with their corresponding siRNAs.

The siRNA sequences used were as follows: Ctrl_Allstars_1 (undisclosed by QIAGEN), Mm_Cdh1_1 (5'-ACGGAGGAGAACGGTGGTCAA-3'), Mm_Cdh1_6 (5'-CCGGGACAATGTGTATTACTA-3'), Mm_Catna1_1 (5'-CAGATGGAAATTAATGACCAA-3'), Mm_Catna1_6 (5'-CTGGTAAACACCAATAGTAAA-3'), Mm_Catnb_2 (5'-CAGATAGAAATGGTCCGATTA-3'), Mm_Catnb_3 (5'-CTCACTTGAATAATTACAAA-3'), Mm_Myo10_1 (5'-CAGGACGAAGCCATCAAGATA-3'), Mm_Myo10_4 (5'-AAGCACCAAGCTGATCCTCAA-3').

Mouse embryo work. C57BL/6 wild-type females at 28–32 days of age were superovulated, mated and euthanized by cervical dislocation. Embryos were flushed from oviducts with M2 medium (Merck) and cultured in KSOM + AA (Merck) at 37 °C and 5% CO₂ covered by mineral oil (Sigma). All experiments were performed with preimplantation mouse embryos following Monash University Animal Ethics guidelines. Embryos showing clear signs of abnormal or arrested development were excluded from our experiments following previous criteria^{1,2,16–18}. Purified RNA was diluted in injection buffer (5 mM Tris, 5 mM NaCl and 0.1 mM EDTA) and 0.1–0.3 μ l was microinjected using a FemtoJet (Eppendorf). Embryos were cultured in LabTek chambers (Nunc) at 37 °C and 5% CO₂ in an incubator adapted for the microscope system (Zeiss). To produce mosaic embryos comprising cells expressing two different fluorescent proteins that label filopodia, one cell of a 2-cell-stage embryo was microinjected with memb-mCherry together with Patent Blue V (0.4%, Sigma, 21605) and then the other cell with E-cad-GFP (Supplementary Fig. 2). Patent Blue V allowed visualization of the initially microinjected cell. For immunolabelling, embryos were fixed in 4% paraformaldehyde in DPBS for 30 min, washed in DPBS containing 0.1% Triton X-100, permeabilized for 30 min in DPBS containing 0.25% Triton X-100, incubated in blocking solution (10% fetal bovine serum in DPBS) for 2 h, incubated with primary antibodies in blocking solution overnight at 4 °C, rinsed in DPBS, incubated with Alexa-conjugated species-specific secondary antibodies (Invitrogen) in blocking solution (1:500) for 2 h and rinsed in DPBS. Antibodies used include rat anti-E-cad DECMA-1 (1:100, Sigma, U3254), rabbit anti- α -cat (1:2,000; Sigma C2081), mouse anti- β -cat (1:100, BD Transduction Labs 610154), rabbit anti-Myo10 (1:500, Novus Biologicals, 22430002) and mouse anti- α -tubulin DM1a (1:200, Abcam ab7291). To label F-actin, fixed embryos were incubated with rhodamine-phalloidin (1:500, Molecular Probes, R415) with secondary antibodies in blocking solution, as specified above. For function blocking, we treated non-compacted 8-cell-stage embryos with the DECMA-1 antibody (1:1,500) or control IgG antibody at the same concentration in KSOM + AA. Cytochalasin D (Sigma, C8273) was used at 3 μ g ml⁻¹ or 0.5 μ g ml⁻¹ and nocodazole (Sigma, M1404) at 3 μ g ml⁻¹ in KSOM + AA; control embryos were treated with dimethylsulphoxide in KSOM + AA at 1:1,300 for cytochalasin D and 1:8,000 for nocodazole experiments. No differences in filopodia formation and compaction phenotypes were found between embryos treated with dimethylsulphoxide in KSOM + AA at the specified concentrations and those cultured in KSOM + AA alone.

Cell shape and compaction analysis. To quantify the number of cells per embryo that extend filopodia throughout compaction, and the number of neighbouring cells targeted with each filopodia set, we analysed embryos that had been microinjected

with E-cad-GFP and memb-mCherry at the 1-cell stage. To quantify filopodia-related changes in whole cell shape, we first selected time series in which the entire apical surface of a membrane-labelled cell of interest could be visualized throughout. As the embryos spin inside the zona pellucida, it was not possible to follow a single cell long enough to measure aspect ratio changes throughout an entire cycle of filopodia extension and retraction. Therefore, a 3D reconstruction of the embryo was created using Zen software (Zeiss) and individual frames were selected immediately before and after filopodia extension or retraction. The circumference of the filopodia-forming cell was traced at each time point using ImageJ software and the aspect ratio was calculated by dividing the maximum diameter of the cell by the minimum diameter of the cell (d_{\max}/d_{\min}). We determined the ability of a cell to integrate into the compacting embryo by analysing differential interference contrast (DIC) images following previous criteria^{16,18}. Under normal conditions, cells in compacting embryos appear flattened with partially obscured cell outlines that become fully obscured as compaction completes. Simultaneously, the aspect ratio of a compacting cell increases as it elongates its apical membrane and integrates into the compacted mass. We measured the aspect ratio of membrane-labelled cells in treated and control embryos at the 12- to 16-cell stage, when normal embryos become fully compacted.

Confocal and two-photon excitation imaging of filopodia in live embryos.

We imaged live embryos using a Zeiss LSM 780 laser scanning confocal microscope and avalanche photodiodes of the Confocor 3 module (Zeiss) to avoid unwanted phototoxicity and photobleaching. A water-immersion C-Apochromat $\times 40/1.2$ NA objective was used for all experiments except for laser ablations, where a $\times 63/1.4$ NA objective was used. Fusion proteins containing Cerulean were imaged with 488 nm light; GFP with 488 nm light; and RFP, mCherry and mPlum with 561 nm and appropriate filter combinations. DIC was performed using the appropriate slider/prism. Pinhole sizes were adjusted to obtain 2 μ m confocal Z planes. 3D views of the embryos were obtained using Zen (Zeiss) and Imaris (Bitplane) software. We determined whether cells divided symmetrically, allocating daughter cells to the outer and inner positions of the embryo, or asymmetrically, contributing daughter cells only to outer positions, using previously established criteria^{16–18}. Briefly, outer cells have larger membrane regions exposed to the zona pellucida surrounding the embryo, whereas inner cells are internalized within the embryo and are not exposed to the zona pellucida. To visualize all cells of the same live embryo, we used a Zeiss LSM 780 laser scanning microscope with a reflected light BiG GaAsP NDD module (Zeiss) and a water-immersion C-Apochromat $\times 40/1.2$ NA objective. We excited the E-cad-GFP fusion protein expressed by all cells using a multiphoton Ti:sapphire laser (Chameleon, Coherent) tuned to 920 nm and set to $\sim 3\%$ transmission, and collected emitted light with a 500–550 nm filter, with 1 μ m intervals along the z axis. We analysed the distribution of filopodia extended by individual cells of the embryos using 3D views of the confocal and two-photon excitation (2PE) data. To visualize all filopodia in the same embryo we generated several cropped versions of the 3D 2PE data, which allowed us to rotate and determine the presence and distribution pattern of all filopodia in each cropped data set. For the experiments in Fig. 5a, we excluded from the analysis cells showing no filopodia because we cannot distinguish whether these cells lack filopodia as a result of the effect of a molecular manipulation, or because of the natural lack of filopodia by 39–44% of cells in the embryo. For the experiments in Fig. 5i and Supplementary Figs 5 and 6, detached filopodia were scored by comparative analysis of 3D reconstructions for both DIC and fluorescence channels, with their matching single plane series along the Z stack. Detached filopodia were readily distinguishable when rotating the 3D views because under normal conditions filopodia are completely attached to the neighbouring cell membrane throughout their entire length. For the experiments in Fig. 7, we determined whether cells extending filopodia belonged to a second- or third-cleavage blastomere type by performing confocal time-lapse imaging with a 30 min interval from the 4- to the 8- cell stage. Second- and third-cleavage cells were readily distinguished by tracking all cells throughout divisions and also by size differences, as second-cleavage cells are approximately twice larger than third-cleavage cells and this difference can be readily observed in 3D views of the embryos. For the rescue experiments in Supplementary Fig. 5, the fluorescence intensity of E-cad-GFP and GFP-Myo10 were detectable in the injected cells, but at reduced levels compared with untreated embryos expressing equal concentrations. This suggests that despite the fact that the siRNAs target some of the E-cad-GFP and GFP-Myo10 used to rescue the compaction phenotype, there remains some protein to obtain a rescue effect.

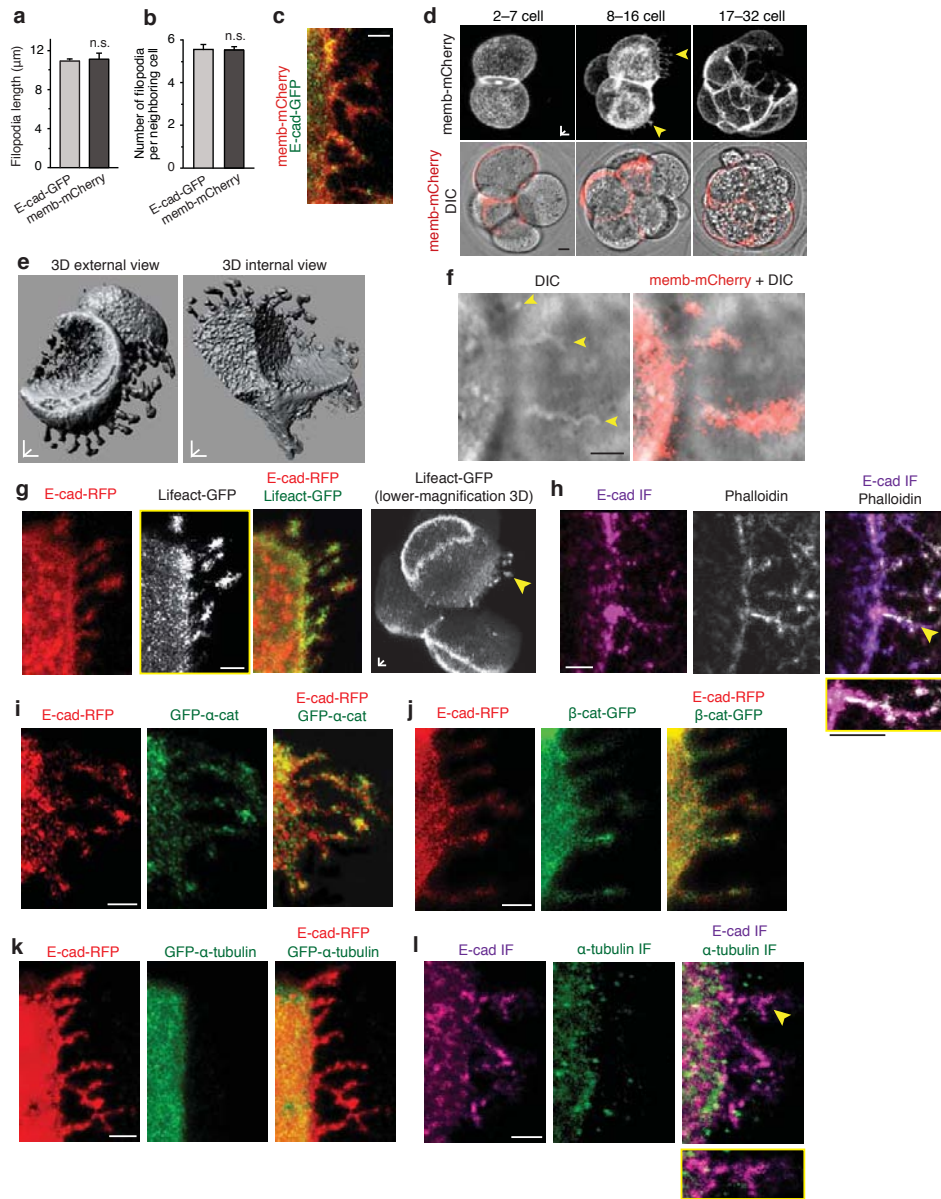
Laser ablations. Laser ablations were performed using a Zeiss oil-immersion ultraviolet-visible-infrared Plan-Apochromat $\times 63/1.4$ NA objective at 2 \times digital magnification on embryos expressing memb-mCherry to visualize the cell membrane and filopodia. Fluorescence and transmitted light images were acquired using one-photon excitation (561 nm light) before and after ablation with an interval of <30 s. A multiphoton Ti:sapphire laser (Chameleon, Coherent) tuned

to 790 nm was used to perform ablations. For technical reasons we were unable to ablate all of the filopodia extended by a cell. Thus, we selected single filopodia extending orthogonal to the plane of imaging. For filopodia ablation, a rectangular region of interest (ROI) of $3 \times 1 \mu\text{m}$ lateral dimensions was targeted to the filopodium and scanned twice with the multiphoton laser set at 20% transmission (76 mW as measured at the back end of the objective) with a pixel dwell time of 12.6 μs . In some cases, embryo movement caused mistargeting of the ablation and/or damage to the neighbouring cell and these experiments were excluded from analysis. For adherens junction ablations, a ROI of similar dimensions was positioned along the adherens junction. We confirmed that the use of 20% laser transmission was sufficient to produce an ablation by the lack of fluorescence recovery within the ROI (Supplementary Fig. 4). Using 5% laser transmission did not cause an ablation, just photobleaching, and accordingly mCherry fluorescence recovered over time within the ROI. The normalized fluorescence recovery graph was generated using ImageJ and GraphPad Prism 5 software. For the analysis, raw data were first adjusted by background subtraction at each time point, corrected to a time-matched ROI in the same embryo that had not been ablated and then normalized to the background-subtracted pre-ablation values. To determine local changes in cell shape we used single confocal planes of memb-mCherry-labelled cells extending filopodia. Images were taken immediately before and within 30 s following ablation. The membrane region adjacent to the filopodia base was traced using two straight lines and the angle between these lines was calculated using ImageJ software.

Statistical analyses. All statistical analyses were performed with GraphPad Prism 5 software. A paired or unpaired, two-tailed Student's *t*-test was used as appropriate, with data presented as mean \pm standard error of the mean (s.e.m.); for the strength of the *P* value estimates, we always assumed unequal variances. For analysis of defects in compaction phenotypes (Supplementary Fig. 5), all embryos derived from at least 3 experimental replicates were combined and divided into two phenotypic groups for each treatment, as either undergoing normal or abnormal compaction.

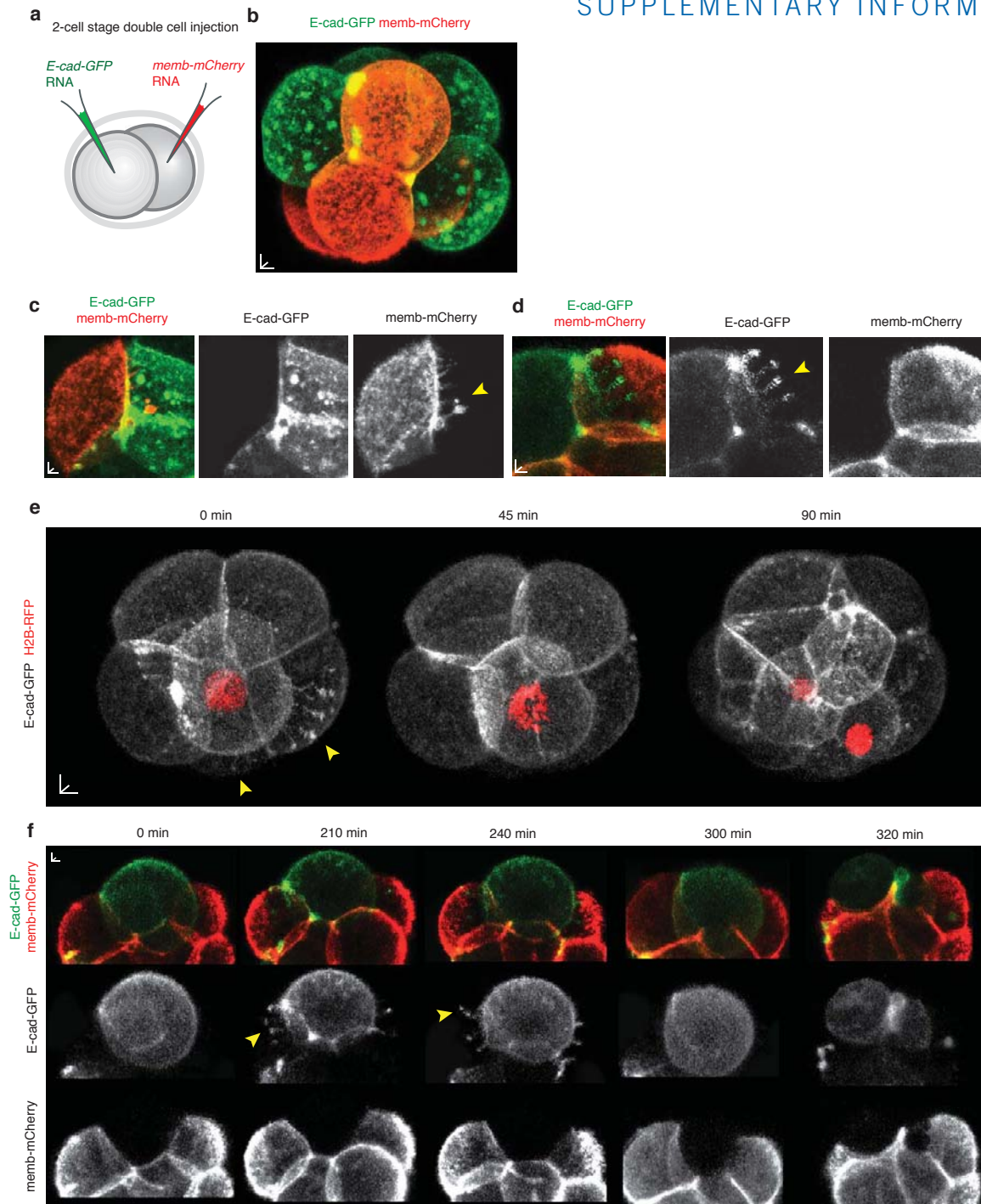
We compared a specific treatment with its corresponding control by creating a 2×2 contingency table, consisting of the two phenotypic groups and the two treatments, to be able to calculate the corresponding *P* value by Fisher's exact test. The investigators were blinded to the group allocation (that is, test versus control) during all experiments, and also for all outcome assessments during the data analysis process. In brief, different treatments or conditions were marked with neutral labels, which were not known to the investigator at the time of performing the experiments or the analysis. The exception was for the data shown in Fig. 4, because for this experiment we knew a priori through observation whether we were analysing changes in membrane angles resulting from laser ablation of either the filopodium or the adherens junction. For Fig. 2f, the number of filopodia (*n*) used per condition was: 21 for 1PE, and 17 for 2PE. For Fig. 2g, the number of embryos (*n*) used per condition was: 10 for 1PE, and 12 for 2PE. For Fig. 2h, the number of cells (*n*) used per condition was: 18 for 1PE, and 15 for 2PE. For Fig. 2i, the number of cells (*n*) used per condition was: 23 for 1PE, and 24 for 2PE. For Fig. 5a, the number of cells (*n*) used per treatment was: 61 for control siRNA, 18 for E-cad siRNA, 20 for α -cat siRNA, 29 for β -cat siRNA, 18 for Myo10 siRNA, 11 for E-cad-RFP, 16 for E-cad Δ ECD-RFP, 15 for GFP-Myo10, and 24 for GFP-Headless. For Fig. 5b, the number of cells (*n*) used per treatment was: 17 for control siRNA, 18 for E-cad siRNA, 19 for α -cat siRNA, 14 for β -cat siRNA, 21 for Myo10 siRNA, 7 for E-cad-RFP, 20 for E-cad Δ ECD-RFP, 9 for control antibody, 17 for E-cad antibody, 13 for 4 h cytochalasin D ($0.5 \mu\text{g ml}^{-1}$), 12 for 4 h wash, 16 for GFP-Myo10, and 23 for GFP-Headless. For Fig. 5h, the number of filopodia (*n*) used per treatment was: 14 for control antibody, 21 for E-cad antibody, 23 for 4 h cytochalasin D ($0.5 \mu\text{g ml}^{-1}$), and 22 for 4 h wash. For Fig. 5i, the number of filopodia (*n*) used per treatment was: 24 for control antibody, 46 for E-cad antibody, 111 for 4 h cytochalasin D ($0.5 \mu\text{g ml}^{-1}$), and 36 for 4 h wash. The experiments were not randomized, and no statistical method was used to predetermine sample size. Reproducibility of all results was confirmed by independent experiments. All experiments shown in all figures were repeated at least 3 times (there were no limitations in repeatability).

DOI: 10.1038/ncb2875



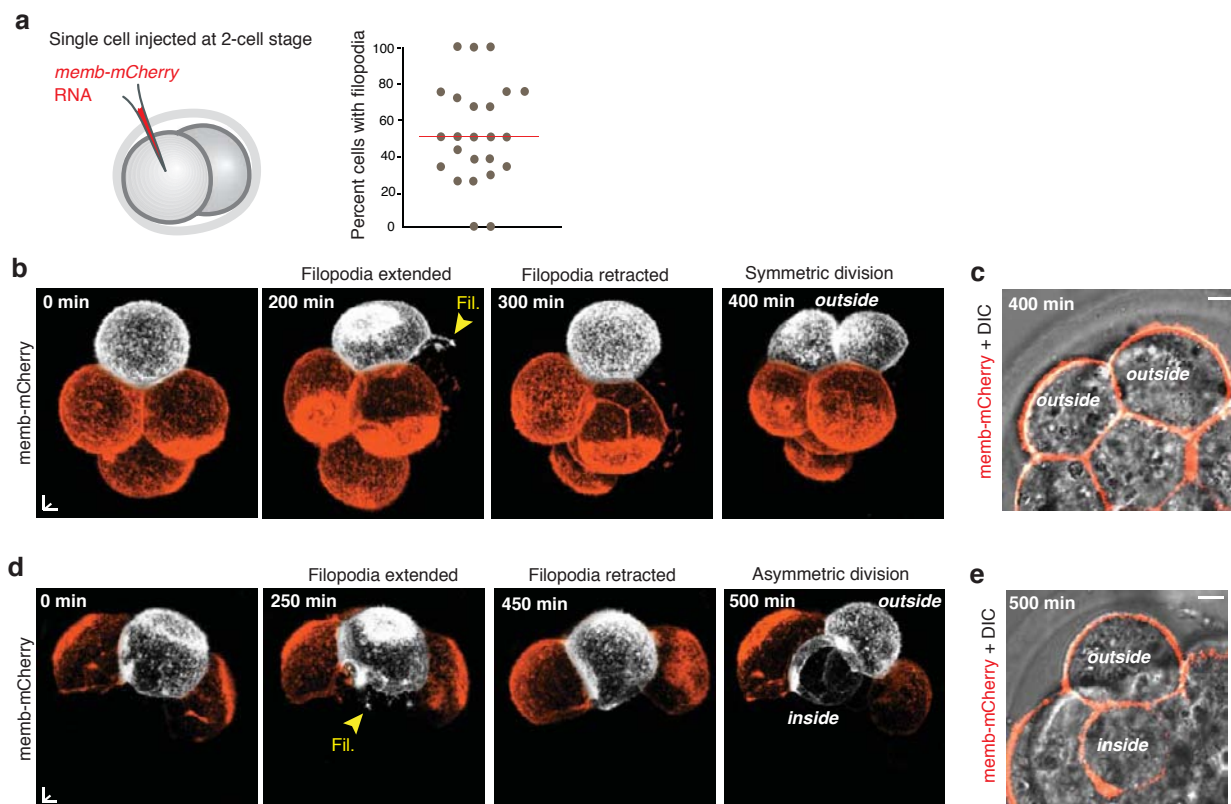
Supplementary Figure 1 Characterization of filopodia with membrane-targeted mCherry, DIC, F-actin, α -cat and β -cat. **a, b**, Filopodia length and number in embryos microinjected with E-cad-GFP or memb-mCherry RNA. In **a**, $n = 21$ filopodia for E-cad-GFP; 23 for memb-mCherry. In **b**, $n = 18$ cells for E-cad-GFP; 12 for memb-mCherry. **c**, E-cad-GFP colocalizes with memb-mCherry in filopodia. **d**, Representative example of live embryos labelled with memb-mCherry in half of the cells at different developmental stages. Filopodia (arrowheads) are only detectable during compaction (8- to 16-cell stage). $n = 20$ embryos. **e**, Three-dimensional surface renders of embryo from Fig. 1e. Filopodia extend from the border membrane region between the AJ and apical domain of the filopodia-forming cells on top of the neighbouring cell apical membrane (not labelled in this example). **f**, Visualization of filopodia (arrowheads) by DIC. Images in **g, i, j** and **k** are from live 8-cell stage embryos microinjected into one cell at the 2-cell stage with RNAs to express

E-cad-RFP and Lifeact-GFP (**g**), GFP- α -cat (**i**), β -cat-GFP (**j**) and GFP- α -tubulin (**k**). Images in **h, l** are from non-injected, fixed 8-cell stage embryos, double-stained with E-cad antibodies (E-cad IF) and rhodamine-phalloidin (**h**) or α -tubulin antibodies (**l**). **g**, E-cad-RFP-labelled filopodia are enriched in F-actin revealed by Lifeact-GFP fluorescence in a live embryo. Arrow shows detection of filopodia in a low-magnification 3-dimensional view of the embryo. Yellow-boxed image shows higher-magnification view of the filopodia. **h**, Co-localization of E-cad and rhodamine-phalloidin. **i-k** E-cad-RFP also co-localizes with α - and β -cat fused to GFP (**i, j**), but not with GFP- α -tubulin (**k**) in filopodia. **l**, E-cad does not co-localize with α -tubulin in filopodia. Yellow-boxed images in **g, h** and **l** show higher-magnification views to better visualize some of the filopodia. n.s., not significant by *t* test. Error bars represent s.e.m. Statistics source data for **a** and **b** can be found in Supplementary Table S1. Horizontal and orthogonal scale bars, 5 μ m.



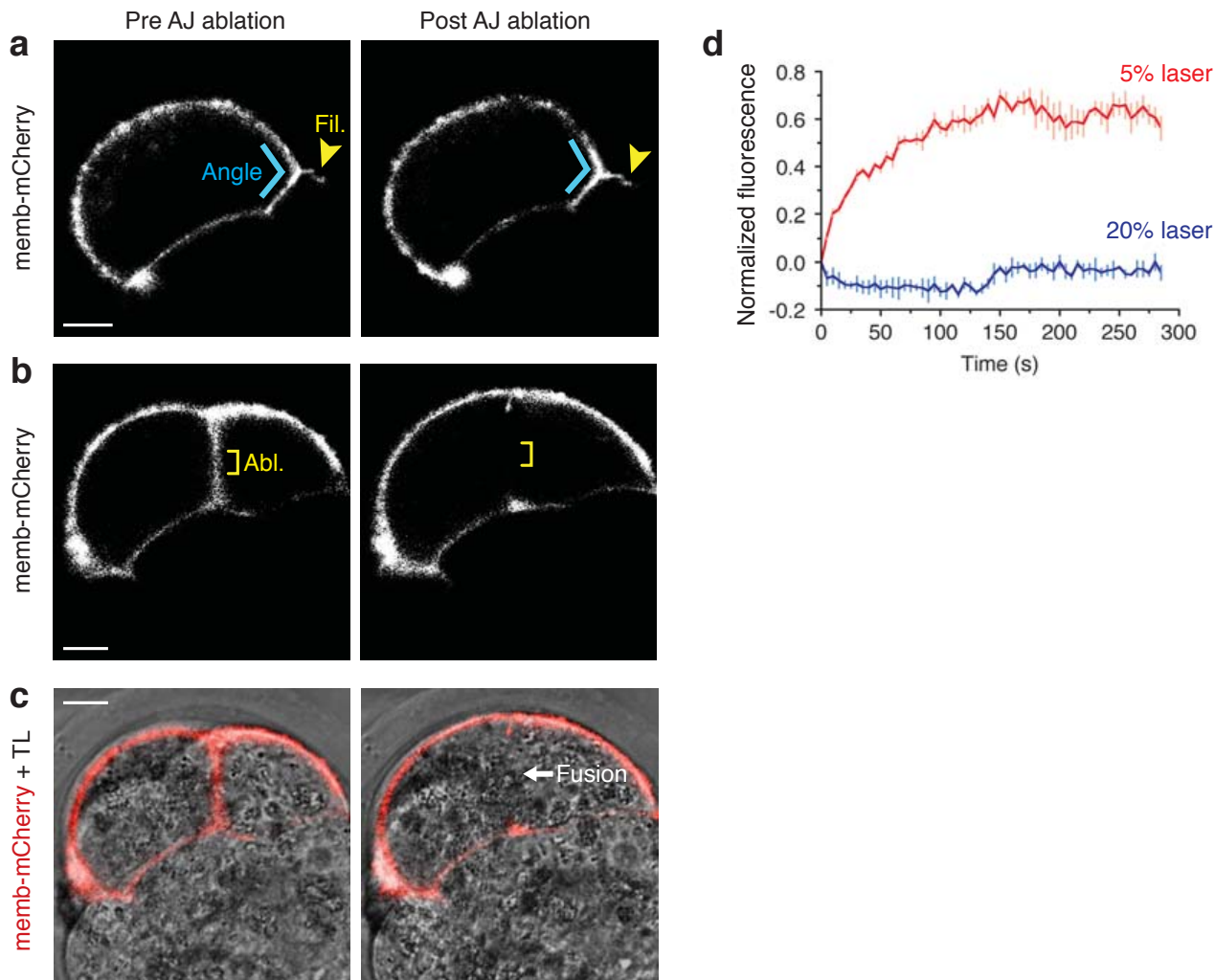
Supplementary Figure 2 Filopodia do not extend simultaneously between neighbouring cells and they retract before cell division. **a**, Schematic experimental design. Each cell of a 2-cell stage embryo is microinjected with either E-cad-GFP or memb-mCherry. **b**, Representative example of a live, early 8-cell stage embryo, microinjected at the 2-cell stage as described in **a** comprising four E-cad-GFP-positive and four memb-mCherry-positive cells. **c**, Representative example of a cell expressing memb-mCherry extending filopodia on top of an E-cad-GFP-positive cell. **d**, Representative converse situation to that in **c**, showing a cell expressing E-cad-GFP extending filopodia on top of a memb-mCherry-positive cell. Note that in **c** and **d** the cell receiving filopodia does not extend reciprocal filopodia onto the filopodia-forming cell. Analysis of multiple embryos manipulated as described in this figure revealed complete absence of reciprocal filopodia extension between cells of the embryo ($n = 8$ embryos). **e**, Selected 3-dimensional reconstructions of a live embryo (8-cell stage) microinjected

at the 1-cell stage with E-cad-GFP and H2B-RFP RNAs. For simplicity of illustration, the H2B-RFP signal is only shown for the cell of interest. The H2B-RFP-labeled cell is a filopodia-forming cell, as at time 0 min it is extending filopodia (arrows) on top of its neighbours. Prior to undergoing division the cell retracts its filopodia. The mitotic events can be followed by condensation of the H2B-RFP-labeled chromatin (right panel) and the divisions of the two daughter nuclei (left panel). As illustrated in these examples, we never observed filopodia from neighbouring cells extending on top of a cell engaged in cell division ($n = 30$ cells in 15 embryos). **f**, The same pattern of filopodia retraction prior to division of the filopodia-forming cell is obtained when viewing embryos in which filopodia-forming cells and their neighbours are labeled with either E-cad-GFP or memb-mCherry microinjected as described in **a**. Note that also as illustrated in this example, neighbouring cells (red) do not extend filopodia on top of the cell engaged in division (green). Orthogonal scale bars, 5 μm .



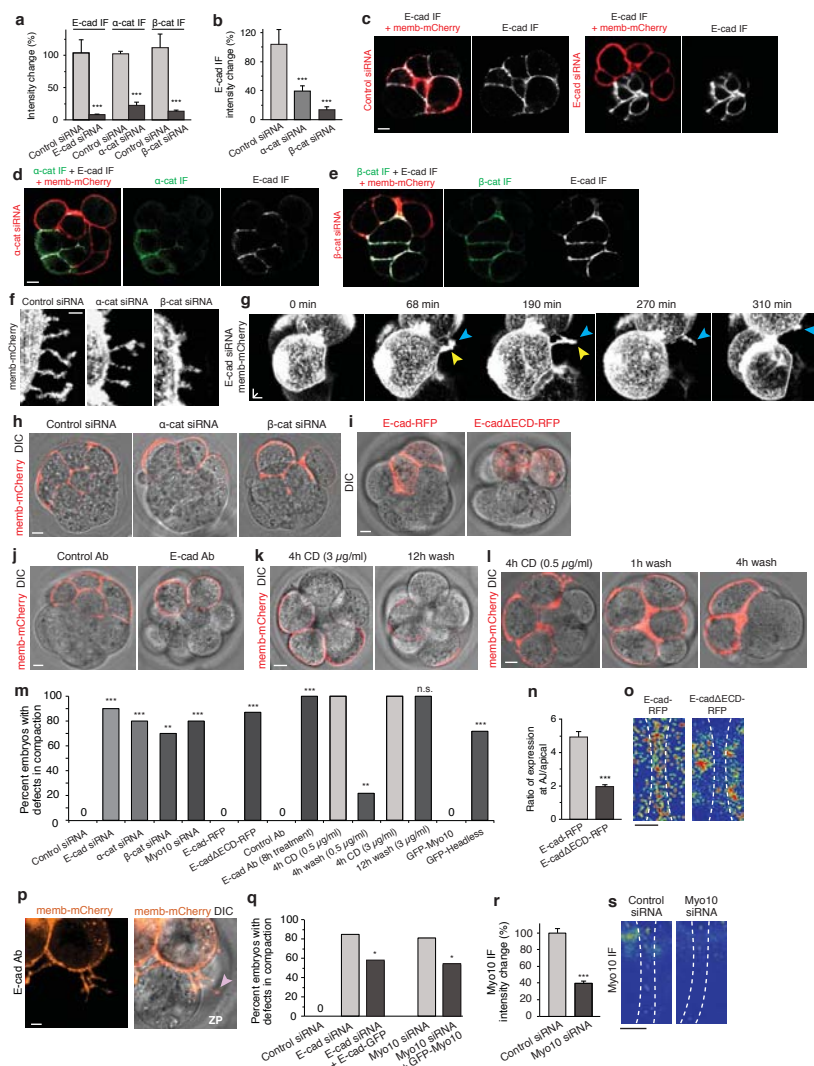
Supplementary Figure 3 Two-cell stage blastomeres contribute filopodia-forming cells to variable extents. **a**, Schematic representation of the experimental approach (left panel). Only one cell was microinjected at the 2-cell stage with *memb-mCherry* and the contribution of filopodia-forming cells by that single cell was then assessed during compaction. Each data point in the graph represents a single embryo. The scattered distribution pattern of the data suggests no obvious systematic contribution of filopodia-forming cells by the original 2-cell stage blastomeres. Individual 2-cell

stage blastomeres can contribute filopodia-forming cells to variable extents ($n = 24$ embryos). **b–e**, Selected frames over time show a filopodia-forming cell (in white) undergoing symmetric (**b**) or asymmetric (**d**) division ($n = 13$ cells in 11 embryos). During symmetric division the two daughter cells are allocated to the outer, extraembryonic regions (**c**), while in asymmetric division, one of the daughter cells becomes internalized to the pluripotent region (**e**). Embryos were microinjected with *memb-mCherry* as described in **a**. Arrowheads depict filopodia. Horizontal and orthogonal scale bars, 5 μm .



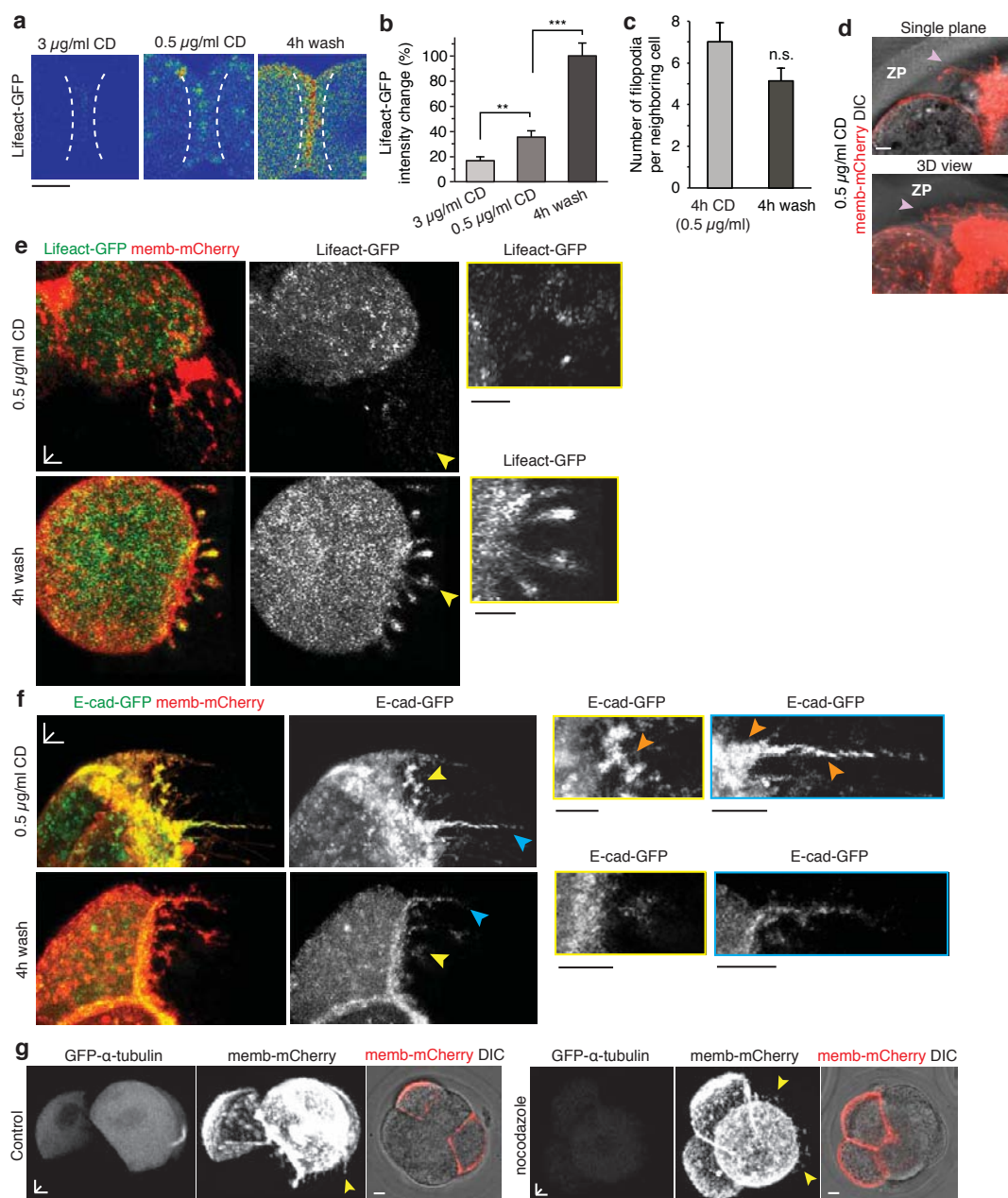
Supplementary Figure 4 Extensive AJ ablations do not alter the shape of the apical border adjacent to filopodia. **a**, Immediately following AJ laser ablation (yellow brackets in **b**), the angle of the cell membrane (blue angle) in the apical border region where filopodia extended (yellow arrowheads) remains unchanged. **b**, A different focal plane of the same cell shown in **a** depicts the AJ region where laser ablation was performed (yellow brackets). **c**, Transmitted light imaging at the same focal plane as **b** shows that the two adjacent cells

fused (white arrow) following ablation. Embryos were microinjected with memb-mCherry into one cell at the 2-cell stage. **d**, Lack of fluorescence recovery following laser ablation. Cells expressing memb-mCherry were ablated at the AJ with 20% laser intensity transmission. Fluorescence recovery in the irradiated region is observed with 5%, but not 20% transmission indicating complete ablation is achieved with 20%. Vertical lines represent mean \pm s.e.m ($n = 3$ cells from 3 different embryos per treatment). Scale bars, 5 μ m.



Supplementary Figure 5 Expression and manipulation of endogenous E-cad, α -cat, β -cat, F-actin and Myo10. **a**, Efficient knockdown of endogenous E-cad, α -cat, β -cat by microinjection of siRNAs into one cell of the embryo at the 2-cell stage ($n = 18$ cells for Control siRNA, 6 for E-cad siRNA, 15 for α -cat siRNA, and 8 for β -cat siRNA), as measured by immunofluorescence (IF). **b**, Knockdown of α - or β -cat significantly downregulates E-cad protein ($n = 6$ cells for Control siRNA, 15 for α -cat siRNA, and 8 for β -cat siRNA). In **a** and **b**, a scrambled control siRNA did not alter protein levels; non-injected cells were used as internal control. $***P < 0.001$ by t test. Error bars represent s.e.m. **c–e**, Selected single plane images show the knockdown effects measured in **a** and **b**. **f**, Knockdown of endogenous α - and β -cat results in fewer filopodia. **g**, The fewer filopodia that still form in cells microinjected with E-cad siRNA display overall elongation-retraction dynamics similar to control cells. Selected time frames from an embryo microinjected with E-cad siRNA and memb-mCherry into one cell at the 2-cell stage. Two neighbouring cells extend a single filopodium each on top of a non-injected cell (unlabeled in this example). Yellow and blue arrows distinguish each filopodium. Note that the time window used to image these cells was sufficient to capture the division of the lower cell extending the yellow-marked filopodium following filopodia retraction. The timing of filopodia elongation and retraction are overall similar to those recorded for control cells in Fig. 1f. **h–m**, Molecular manipulations of filopodia components prevent cells from integrating into the compacting embryo. **h, i**, Cells microinjected with siRNAs against α - or β -cat (**h**) or with E-cad Δ ECD-RFP (**i**) fail to integrate into the compacting embryo and remain rounded. **j–l**, Cells in embryos treated with the E-cad antibody (**j**) or cytochalasin D (CD) at 3 μ g/ml (**k**) or 0.5 μ g/ml (**l**) remain rounded and embryos fail to compact. In **k**, following 3 μ g/ml CD washout embryos fail to extend filopodia and their cells remain

rounded, while following 0.5 μ g/ml CD washout in **l** embryos extend normal-appearing filopodia and resume compaction (see also Fig. 5). In **h** embryos were co-microinjected with memb-mCherry into one cell at the 2-cell stage. In **j–l**, memb-mCherry was injected into half of the cells to visualize filopodia and cell shape. **m**, Percent of embryos displaying defects in compaction when subjected to the different molecular manipulations shown in panels **h–l** and Fig. 5b. $***P < 0.001$; $**P < 0.01$; n.s., not significant by Fisher's exact test (see Methods for a detailed explanation on statistical analyses). **n**, E-cad Δ ECD-RFP does not accumulate at regions where filopodia normally extend. Unlike E-cad-RFP, E-cad Δ ECD-RFP is not enriched at regions where filopodia normally extend. Apical membrane regions of the same embryo were used as internal control ($n = 11$ cells for E-cad-RFP, and 12 for E-cad Δ ECD-RFP). $***P < 0.001$ by t test. Error bars represent s.e.m. **o**, Selected rainbow images represent the changes in expression shown in **n**. **p**, Example of detached filopodia in embryo treated with the E-cad antibody DECMA1. Representative Z projection showing a clearly detached filopodium (arrowhead) projecting outwards from the embryo towards the zona pellucida (ZP). The embryo was microinjected into one cell of the 2-cell stage with memb-mCherry and treated with the DECMA1 antibody. **q**, The defects in compaction caused by the E-cad and Myo10 siRNAs can be rescued by $\sim 27\%$ in the presence of E-cad-GFP or GFP-Myo10, respectively. $*P < 0.05$ by Fisher's exact test. **r**, Efficiency of knockdown with Myo10 siRNAs microinjected into one cell at the 2-cell stage ($n = 12$ cells for Control siRNA, and 11 for Myo10 siRNA), as measured by immunofluorescence (IF). $***P < 0.001$ by t test. Error bars represent s.e.m. **s**, Selected rainbow images show the knockdown effects measured in **r**. Statistics source data for **a**, **b**, **m**, **n**, **q** and **r** can be found in Supplementary Table S1. Orthogonal and horizontal scale bars, 5 μ m.



Supplementary Figure 6 Effects of cytochalasin D and nocodazole treatments. **a**, Representative images of Lifact-GFP fluorescence following treatment with Cytochalasin D (CD). CD at 3 µg/ml largely depletes Lifact-GFP fluorescence. CD at 0.5 µg/ml reduces, but does not completely deplete Lifact-GFP fluorescence. A 4-hour incubation in KSOM+AA (4h wash) restores Lifact-GFP expression only in embryos treated with 0.5 µg/ml CD. **b**, Quantification of Lifact-GFP fluorescence along the cell membrane. In **b**, $n = 22$ cells for 3 µg/ml CD; 15 for 0.5 µg/ml CD; 19 for 4h wash. $***P < 0.001$; $**P < 0.01$ by t test. Error bars represent s.e.m. **c**, Filopodia number per neighbouring cell is not significantly higher in embryos treated with 0.5 µg/ml CD, when compared to that observed after 4h wash. (see Fig. 2 and Supplementary Fig. 1 for comparison with untreated embryos). In **c**, $n = 17$ cells for 4h CD (0.5 µg/ml); 7 cells for 4h wash. n.s., not significant by t test. **d**, Representative examples of detached filopodia in embryos treated with 0.5 µg/ml CD. Upper panel shows a single focal plane, lower panel shows 3-dimensional view. Detached filopodia (arrowheads) often extend away from the embryo and contact the zona pellucida (ZP). **e**, Representative examples of a cell in an embryo treated with 0.5 µg/ml CD

showing Lifact-GFP in the abnormally long and detached filopodia (shown by arrow). Four hours following CD washout cells extend new filopodia showing normal Lifact-GFP fluorescence. Insets show higher-magnification views of the filopodia indicated by arrows, which are comparable to the control situation in Supplementary Fig. 1g. **f**, Representative examples of E-cad-GFP distribution pattern following 0.5 µg/ml CD. E-cad-GFP displays a more punctated clustered pattern throughout the cell membrane and along filopodia. Four hours following CD washout cells extend new filopodia showing normal E-cad-GFP fluorescence distribution. Insets show higher-magnification views of the filopodia indicated by arrows. **g**, Embryos treated with 3 µg/ml nocodazole for 4 hours form normal filopodia and undergo compaction. Images show representative examples of embryos treated with nocodazole, which are indistinguishable from control embryos and undergo normal compaction ($n = 12$ embryos). Note the marked decrease in GFP-α-tubulin fluorescence in the nocodazole-treated embryos. Single focal planes are shown for DIC to appreciate compacted morphology. Statistics source data for **b** and **c** can be found in Supplementary Table S1. Horizontal and orthogonal scale bars, 5 µm.

Supplementary Video Legends

Supplementary Video 1 Filopodia dynamics during mouse embryo compaction. Time-lapse imaging of a representative embryo during compaction shows two cells extending filopodia, which then fully retract before cell division. The embryo was microinjected with memb-mCherry into one cell at the 2-cell stage. Orthogonal scale bar, 5 μm .

Supplementary Video 2 E-cad-labelled filopodia retract to the filopodia-forming cell. Time-lapse imaging of a representative embryo during compaction shows a cell (left) with E-cad-GFP-expressing filopodia extended onto its E-cad-GFP-labelled neighbouring cell (right). The long finger-like processes clearly retract and return to the membrane apical border region where filopodia initially attached (left). Orthogonal scale bar, 5 μm .

Supplementary Video 3 Filopodia retraction occurs before cell division. Time-lapse imaging of a representative embryo during compaction shows two cells retracting their memb-mCherry-labelled filopodia just prior to division. H2B-Cerulean-labelled nuclei show chromatin condensation and chromosome separation at the time when filopodia start to retract. Orthogonal scale bar, 5 μm .